nature portfolio

Peer Review File

Efficient thermal management of electronic devices by constructing interlayer phonon bridges

Corresponding Author: Professor Guangming Tao

Parts of this Peer Review File have been redacted as indicated to remove third-party material.

This file contains all reviewer reports in order by version, followed by all author rebuttals in order by version.

Version 0:

Reviewer comments:

Reviewer #1

(Remarks to the Author)
This manuscript proposes a honeycomb-gel densification strategy to construct a bi-directional thermal conduction paths within a layered structure. Significant enhancement in both in-plane and through-plane thermal conductivities are found in the aramid nanofiber/boron nitride nanosheets (ANF/BNNS) film. This work is interesting and provides a new approach to improving the through-plane thermal conductivity in thin films, advancing their practical applications in heat dissipation and radiative cooling. However, some issues have to be addressed before the manuscript can be considered for publication in Nature Communications:

1. Although the thermal conductivity was enhanced through the honeycomb-gel densification, the thermal conductivity is still quite anisotropic with the cross-plane thermal conductivity much lower than the in-plane value. If we take the average thermal conductivity, this is not necessarily better than randomly mixed polymer composites (such as ACS Appl. Mater. Interfaces 2024, 16, 22, 29042–29048) which has isotropic thermal conductivity. Then the advantage of this work needs to be further commented in the context with other polymer composites.

2. While the focus of this work is on bi-directional thermal conxduction in ANF/BNNS films, the measured thermal conductivities values are not convincing enough due to insufficient methodological details. The authors only mention that the thermal diffusivity of the film was measured using LFA 467 NanoFlash system via laser flash method, without any details like mechanisms and sample sizes. There are no uncertainties in the measured values either, which should never be neglected in any measurements.

3. The laser flash method is typically employed to measure the through-plane thermal diffusivity. In some cases, it can be used to measure the in-plane thermal diffusivity with very careful calibrations. For example, people have used it to measure metals and graphite with high in-plane thermal diffusivity [Thermochimica Acta, 2017, 653, 126-132]. However, the in-plane thermal diffusivities of ANF/BNNS films in this work are not as high as those values and might not be accurately captured via laser flash method. In addition, the film thickness will affect the measured in-plane thermal diffusivity via laser flash method, but there is no thickness data in this manuscript. The authors need to compare laser flash method with other commonly used methods like 3-omega method [Journal of applied physics, 1999, 86(7), 3959-3963] and transient thermal grating method [Nano Letters, 2021, 9, 3708–3714] and thoroughly justify their results on thermal diffusivities (especially in-plane ones) via laser flash method.

4. There are no density and specific heat capacity data in the manuscript which are used to calculate thermal conductivity. The authors only claim specific heat capacity was evaluated via DSC measurements, without showing the DSC curves. However, DSC method is tricky for extracting specific heat capacity data as the data can be greatly overestimated if the contact of the measured sample and instrument is not good enough. The authors need to demonstrate that their enhanced thermal conductivity data are not artifacts of overestimated specific heat capacity values.

5. In Fig. 6d and Fig. S19, why do the temperature differences between RgD and HgD films at radiation intensities of 50 mW/cm^2 and 200 mW/cm^2 increase with time, while those at 100 and 150 mW/cm^2 decrease?

6. Several abbreviations, such as DSC and DTG, are used without being defined.

Reviewer #2

(Remarks to the Author)
I co-reviewed this manuscript with one of the reviewers who provided the listed reports. This is part of the Nature Communications initiative to facilitate training in peer review and to provide appropriate recognition for Early Career Researchers who co-review manuscripts.

Reviewer #3

(Remarks to the Author)
This manuscript presents a novel honeycomb-gel densification (HgD) strategy to enhance the through-plane thermal conductivity in layered film-based thermal management materials (f-TMMs), by introducing interlayer phonon bridges via a carefully controlled freeze-casting and densification process. The integration of boron nitride nanosheets (BNNS) and aramid nanofibers (ANF) results in a bi-directional thermal conduction network, with reported enhancements in through-plane thermal conductivity surpassing many existing BNNS-based films. Additionally, the paper suggests a potential application in passive radiative cooling, demonstrating a temperature reduction of up to 10°C under solar irradiation.

While the work presents a promising approach with some strong experimental results, several critical aspects require further clarifications or study:

1. The process of freeze casting followed by gel densification is central to the study. How reproducible is this fabrication method? Are there any potential challenges in maintaining structural consistency across different batches?

2. The paper describes unidirectional freezing to form a honeycomb-like skeleton. How sensitive is this structure to variations in freezing rate, solvent choice, or environmental conditions?

3. How does the applied pressure during densification affect the final film morphology and thermal performance? Is there an optimal pressure range that was determined experimentally?

4. The anisotropy in thermal conductivity is discussed, with higher values in-plane compared to through-plane. How do the observed values align with theoretical predictions based on phonon transport models?

5. The discussion of interfacial phonon scattering suggests that ANF improves phonon transmission across BNNS layers. Are there any direct measurements of interfacial thermal resistance to support this hypothesis?

6. The authors mention that the films exhibit flexibility. How does mechanical flexibility affect thermal performance, as well as durability in application?

7. The authors showed the structural difference in the top view and the side view of the HgD ANF/BNNS film in Fig. 3(a,a',b,b'). It indicates different heat flow pathways in two directions in the in-plane, x and y, respectively, following the axis label in Fig. 3g. How does such structural difference affect the heat transfer in the x and y-direction? If a measurement technique that can distinguish the thermal conductivities in the two in-plane directions is not accessible, the author can visualize and demonstrate the heat conduction in the two directions using setups similar to those shown in Fig. 5(a,b,e,f) and discuss the results.

8. How were the uncertainties in the thermal conductivity measurements analyzed? Error bars are missing in Fig.4(a,c).

9. In Fig. 5f, is the top and bottom row showing the thermal images for RgD ANF/BNNS film and HgD ANF/BNNS film, respectively? Adding labels would avoid confusion for the readers.

10. The authors briefly mentioned that they used insulating polystyrene foams and transparent polyethylene films to mitigate heat conduction and convection for the outdoor test. From the photo of the outdoor setup in Fig. 6g, I assume the polyethylene film covers the top of the setup. Wind can still cause strong forced convection for heat loss from the setup, which leads to unstable measurements. Tall wind shields around the setup may be a better option.

Version 1:

Reviewer comments:

Reviewer #1

(Remarks to the Author)
They have addressed my comments.

Reviewer #2

(Remarks to the Author)
I co-reviewed this manuscript with one of the reviewers who provided the listed reports. This is part of the Nature Communications initiative to facilitate training in peer review and to provide appropriate recognition for Early Career Researchers who co-review manuscripts.

Reviewer #3

(Remarks to the Author)
The authors have addressed my comments adequately and I support its publication.

Response to Reviewer Comments

Reviewer #1 (Remarks to the Author):

This manuscript proposes a honeycomb-gel densification strategy to construct a bi-directional thermal conduction path within a layered structure. Significant enhancement in both in-plane and through-plane thermal conductivities are found in the aramid nanofiber/boron nitride nanosheets (ANF/BNNS) film. This work is interesting and provides a new approach to improving the through-plane thermal conductivity in thin films, advancing their practical applications in heat dissipation and radiative cooling. However, some issues have to be addressed before the manuscript can be considered for publication in Nature Communications:

Reply: We appreciate your careful examination and helpful suggestion. As suggested, the manuscript has been carefully revised and the relevant changes are highlighted.

1. Although the thermal conductivity was enhanced through the honeycomb-gel densification, the thermal conductivity is still quite anisotropic with the cross-plane thermal conductivity much lower than the in-plane value. If we take the average thermal conductivity, this is not necessarily better than randomly mixed polymer composites (such as ACS Appl. Mater. Interfaces, 2024, 16, 22, 29042-29048) which has isotropic thermal conductivity. Then the advantage of this work needs to be further commented in the context with other polymer composites.

Reply: Thank you for your valuable suggestion. The primary objective of this work is to solve the problem of low through-plane thermal conductivity of layered film-based thermal management materials (f-TMMs) by the honeycomb-gel densification. Currently, to address equipment thermal failure induced by localized overheating, f-TMMs with high in-plane thermal conductivity are extensively utilized to enhance the heat diffusion of point heat sources. These materials exhibit excellent heat homogenization and dissipation performance and play a critical role in addressing the thermal management challenges for high-power devices. Notably, constructing through-plane thermal pathways within the layered f-TMMs is crucial for facilitating heat absorption and transfer along the cross-sectional direction, as well as significantly impacting in-plane thermal diffusion efficiency. Compared to the typically low through-plane thermal conductivity of f-TMMs fabricated using conventional film-forming processes, our honeycomb-gel densification strategy involves compressing an interconnected honeycomb skeleton into a film, thereby establishing a continuous zigzag through-plane phonon bridging network. Consequently, this significantly enhances the through-plane thermal conductivity, providing substantial benefits for the thermal management of high-power electronic devices.

Comparing to the randomly mixed polymer composites like the literature you mentioned (ACS Appl. Mater. Interfaces, 2024, 16, 22, 29042-29048), f-TMMs offer several advantages, include: (1) Ultra-thin thickness, enabling seamless integration into the heat dissipation systems of microelectronic devices. (2) High in-plane thermal conductivity facilitates rapid heat diffusion away from localized point heat sources. Enhancing through-plane thermal conductivity can further improve the efficiency of in-plane heat dissipation. (3) Directional heat transfer capability, fulfilling the requirements of intelligent thermal management systems. This work develops a multi-level layered structure within f-TMMs, featuring in-plane high-orientation alignment and vertical phonon bridging, achieved through honeycomb-gel densification. This approach is designed to offer innovative insights and practical solutions for constructing bidirectional heat transfer layer structures.

Revised in Manuscript (Page 2):

…Compared to randomly distributed thermal conductive composites, f-TMMs' ultra-thin thickness, high in-plane thermal conductivity, and directional heat transfer make them crucial for advancing miniaturized and intelligent thermal management systems.

2. While the focus of this work is on bi-directional thermal conduction in ANF/BNNS films, the measured thermal conductivities values are not convincing enough due to insufficient methodological details. The authors only mention that the thermal diffusivity of the film was measured using LFA 467 NanoFlash system via laser flash

method without any details like mechanisms and sample sizes. There are no uncertainties in the measured values either, which should never be neglected in any measurements.

Reply: We apologize for any inadequacies in the details of the thermal conductivity measurements for ANF/BNNS films in this work. To acquire more reliable and convincing values of thermal conductivity, we have implemented the following comprehensive enhancements to the testing process and provided a detailed description.

To determine thermal conductivity (k, W/mK), which is given by $k = \rho \cdot C_p \cdot \alpha$, where ρ, C_p, and α refer to the sample density (g/cm^3), specific heat capacity (J/gK), and thermal diffusivity (mm^2/s). Density ρ was calculated based on the weight and volume. Specific heat capacity C_p was evaluated by using differential scanning calorimeter (DSC Q2000, TA Instruments) measurements. Thermal diffusivity α was measured using a laser flash apparatus (LFA467, NETZSCH). In accordance with the dimensions of the sample tray for the LFA 467 NanoFlash system, the sample to be tested was first cut into a circular disc with a diameter of **25.4 mm** using standard cutter. Subsequently, the thickness (d) of samples were measured using caliper (Figure R1 (Supplementary Fig. 3a)). Graphite was coated on the sample surface to minimize surface reflection and enhance laser energy absorption. At a constant temperature of 25 °C, a laser source emitted a pulse of light instantaneously and uniformly irradiated on the lower surface of the sample. The surface layer absorbed the light energy, causing an instantaneous temperature increase, which acted as the hot end to transfer energy to the cold end via one-dimensional heat conduction. An infrared detector is used to continuously measure the corresponding temperature rise in the center of the upper surface, and the temperature rise versus time curve is obtained (Figure R2 (Supplementary Fig. 4)). Thermal diffusivity values are measured at 3 points on the same specimen. The thermal diffusivity α can be calculated according to the eq. R1:

$$\alpha = \frac{0.1388 d^2}{t_{50}} \tag{R1}$$

where d is the sample thickness and t_{50} is the characteristic time for the sample to heat up to the half of the maximum temperature. The thermal diffusivity values for different samples were calculated using this equation (R1), as illustrated in Figure R3 (Supplementary Fig. 5).

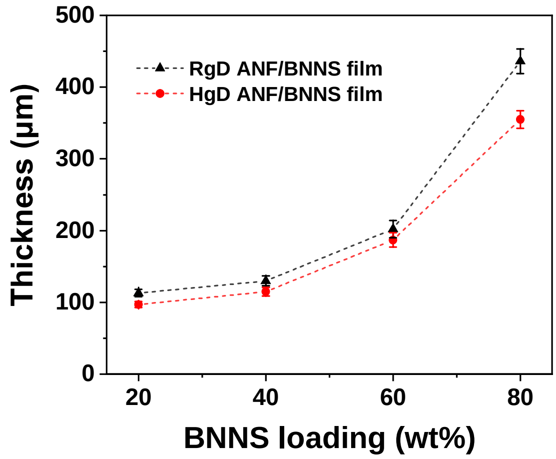

Figure R1 (Supplementary Fig. 3a). Thickness measurements determined by caliper as a function of BNNS loading.

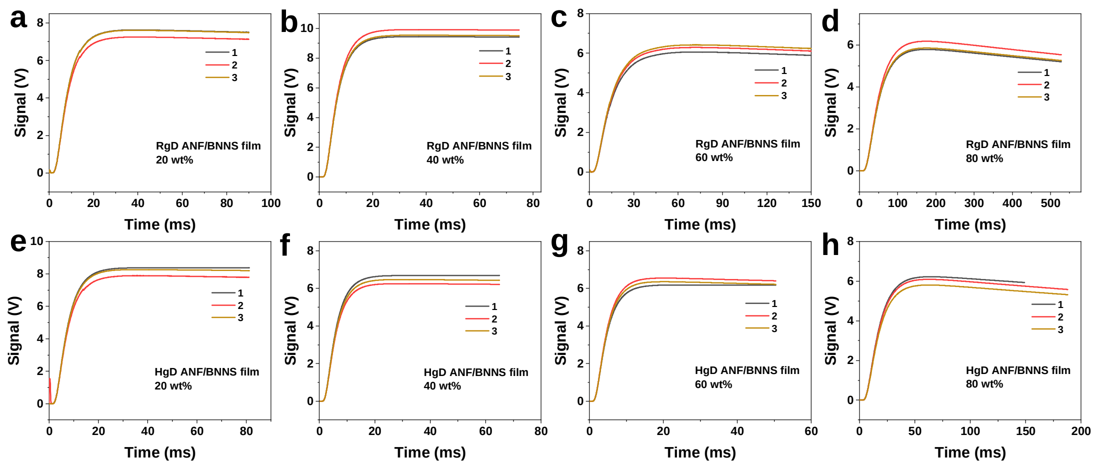

Figure R2 (Supplementary Fig. 4). The curves of the temperature (detector signal) increase over time obtained by the laser flash method.

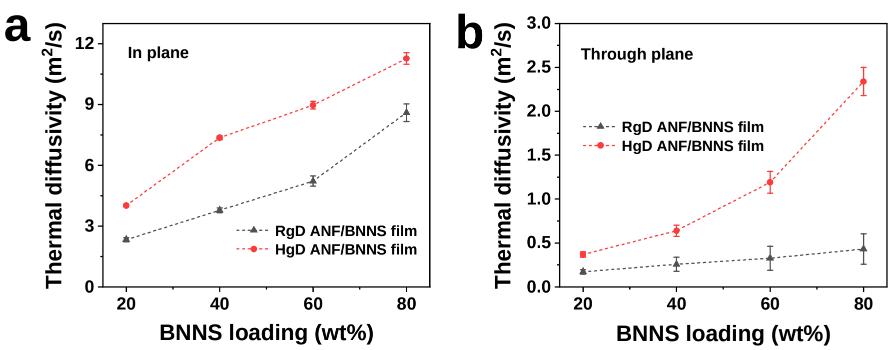

Figure R3 (Supplementary Fig. 5). Thermal diffusivity measured with a laser flash method (LFA467).

Revised in Manuscript (Page 21)

The thermal conductivity (k) of the ANF/BNNS films can be calculated by the equation: $k = \alpha \times C_p \times \rho$, *where thermal diffusivitiy (*α*) of the film was measured using LFA 467 NanoFlash system (NETZSCH, Germany), specific heat capacity (*C_p*) was evaluated by using differential scanning calorimeter (DSC Q2000, TA Instruments) measurements and density (*ρ*) was calculated based on weight and volume measurements. The detailed measurements of* C_p, α, ρ *and sample thickness were shown in Supplementary note 1 (Supplementary Figs. 1-5).*

Revised in Supporting Information (Pages 2-5):

Supplementary note 1

Measurement for Specific heat capacity C_p

Specific heat capacity C_p *was evaluated by using differential scanning calorimeter (DSC Q2000, TA Instruments) measurements. …*

Measurement for Thermal diffusivity α

Thermal diffusivity α *was measured using a laser flash apparatus (LFA467, NETZSCH). In accordance with the dimensions of the sample tray for the LFA 467 NanoFlash system…*

3. The laser flash method is typically employed to measure the through-plane thermal diffusivity. In some cases, it can be used to measure the in-plane thermal diffusivity with very careful calibrations. For example, people have used it to measure metals and graphite with high in-plane thermal diffusivity [Thermochimica Acta, 2017, 653, 126-132]. However, the in-plane thermal diffusivities of ANF/BNNS films in this work are not as high as those values and might not be accurately captured via laser flash method. In addition, the film thickness will affect the measured in-plane thermal diffusivity via laser flash method, but there is no thickness data in this manuscript. The authors need to compare laser flash method with other commonly used methods

like 3-omega method [Journal of applied physics, 1999, 86(7),3959-3963] and transient thermal grating method [Nano Letters, 2021,9, 3708-3714] and thoroughly justify their results on thermal diffusivities (especially in-plane ones) via laser flash method.

Reply: Thank you for your professional comment. The laser flash method for thermal conductivity testing is characterized by its requirement for small sample sizes, rapid measurement speeds, and high precision. This method can measure a wide range of thermal conductivities, ranging from < 0.1 to 2000 W/mK (covering low-conductivity polymers to ultra-high-conductivity diamond). Additionally, it features an extensive temperature measurement range and excellent adaptability to various sample types. By employing suitable fixtures or sample holder plate, it enables the measurement of thermal diffusivity for specialized samples such as multi-layer composites and anisotropic materials, allowing for subsequent calculation of thermal conductivity. Consequently, in the modern field of thermal conductivity testing, the laser flash method is assuming an increasingly significant role. Most researchers have adopted this method to measure the in-plane and through-plane thermal conductivities of layered composite films, such as *Nat. Commun., 2024, 15, 7290, Nat. Commun., 2023, 14, 5342, Adv. Funct. Mater., 2024, 2315851, ACS Nano 2022, 16, 14323-14333*.

Thickness serves as a critical parameter for calculating thermal diffusivity and plays a pivotal role in evaluating thermal conductivity. The thickness of ANF/BNNS film was measured using a caliper, as shown in Figure R1 (Supplementary Fig. 3a). For the RgD film, the thickness increases from 113 μm (20 wt%) to 436 μm (80 wt%). In contrast, the HgD film exhibits a reduction in thickness under the same BNNS content, ranging from 97 μm (20 wt%) to 355 μm (80 wt%), which can be attributed to the densely oriented stacking layer structure formed by honeycomb densification.

Revised in Supporting Information (Supplementary Fig. 3a):

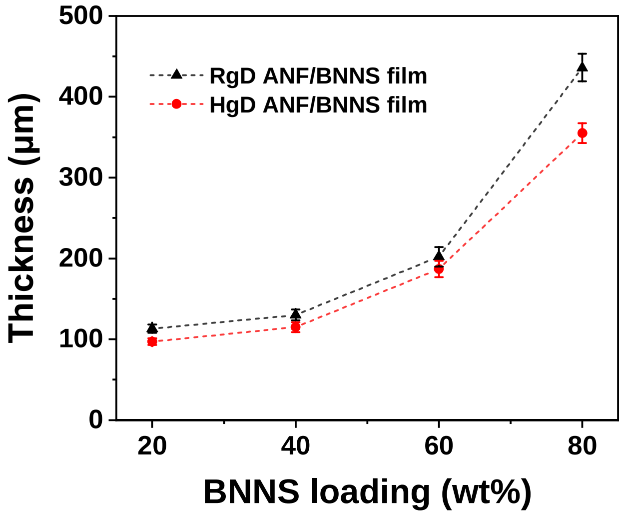

Figure R1 (Supplementary Fig. 3a). Thickness measurements determined by caliper as a function of BNNS loading.

Regarding the suggestion to compare laser flash method with other commonly used techniques like 3-omega method and transient thermal grating method, despite the substantial investment of time and effort, we are very sorry that we haven't found the relevant testing facilities. To evaluate and compare the thermal conductivity, we performed tests on the ANF/BNNS film using a Hot Disk technique (Figure R4a). The principle of Hot Disk measurement is based on the transient heat conduction process and variations in thermal resistance coefficients, enabling it to be widely applicable for investigating the thermal conductivity of various materials. The Hot Disk probe features a thin disc-shaped structure, incorporating double-helical metal sheets within its core and an outer layer composed of high-temperature resistant insulating materials such as polyimide (Figure R4b). During the testing procedure, position the probe at the center of the prepared sample and secure it on the sample holder to ensure measurement stability. According to the Hot Disk test results, the measured thermal conductivity is in good agreement with the laser flash method's through-plane results (Figure R4c and d). This result verifies to a certain extent the reliability of the laser flash method in testing through-plane thermal conductivity.

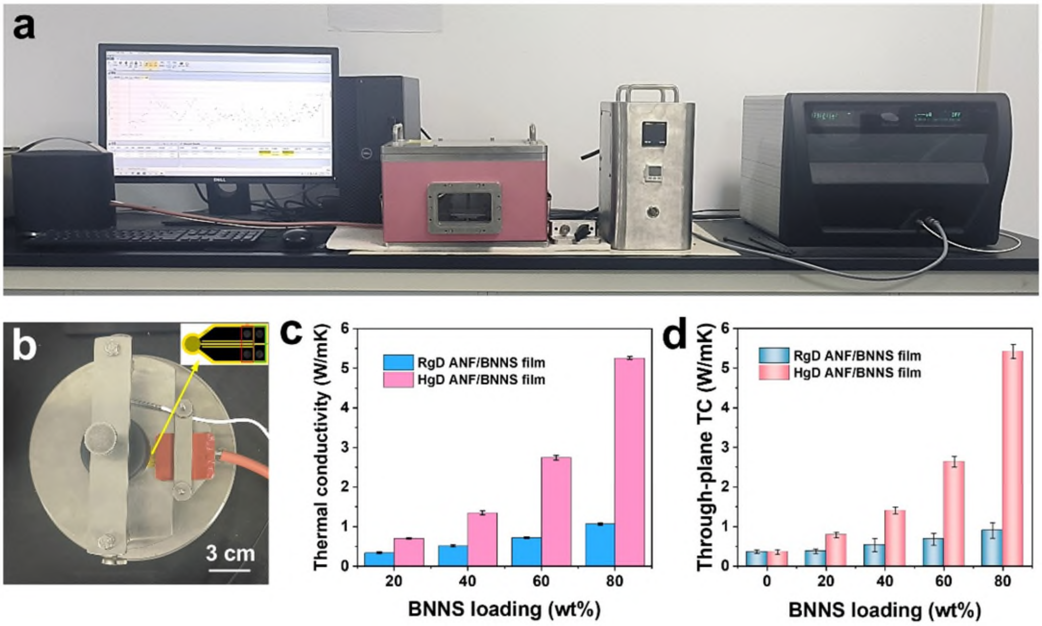

Figure R4. (a) Hot Disk device used for thermal conductivity testing of ANF/BNNS films. (b) Digital images of the probe and sample holder. Comparison of the thermal conductivities of ANF/BNNS films tested by (c) Hot Disk device and (d) laser flash method.

To further assess the in-plane thermal diffusivity using the laser flash method, we performed operations including cutting, splicing and rotating of the HgD ANF/BNNS films, as well as changing the sample holder plate (Figure R5a). Subsequently, we utilized the thermal diffusivity test results in the vertical direction to indirectly infer the in-plane thermal diffusivity. As illustrated in Figure R5a, the samples were cut into rectangles of 12.7 mm × 4 mm × *t*, where *t* is the thickness of the samples perpendicular to the ice crystal growth direction. After a rotation of 90°, the rectangles were spliced into a square of 12.7 × 12.7 × 4 mm^3. Before testing, the samples were sprayed a thin graphite layer after cut and placed on a specific sample holder plate. An infrared detector was employed to continuously monitor the temperature increase at the center of the upper surface, thereby obtaining the temperature rise versus time curves (Figure R5b-e). Compared to the in-plane thermal diffusivity directly measured using laser flash method, the in-plane thermal diffusivity derived from the through-plane testing approach demonstrates a high level of consistency in the results (Figure R5f and g). This suggests that, following meticulous calibration, the in-plane thermal diffusivities and conductivities of the ANF/BNNS films can be reliably determined via laser flash method.

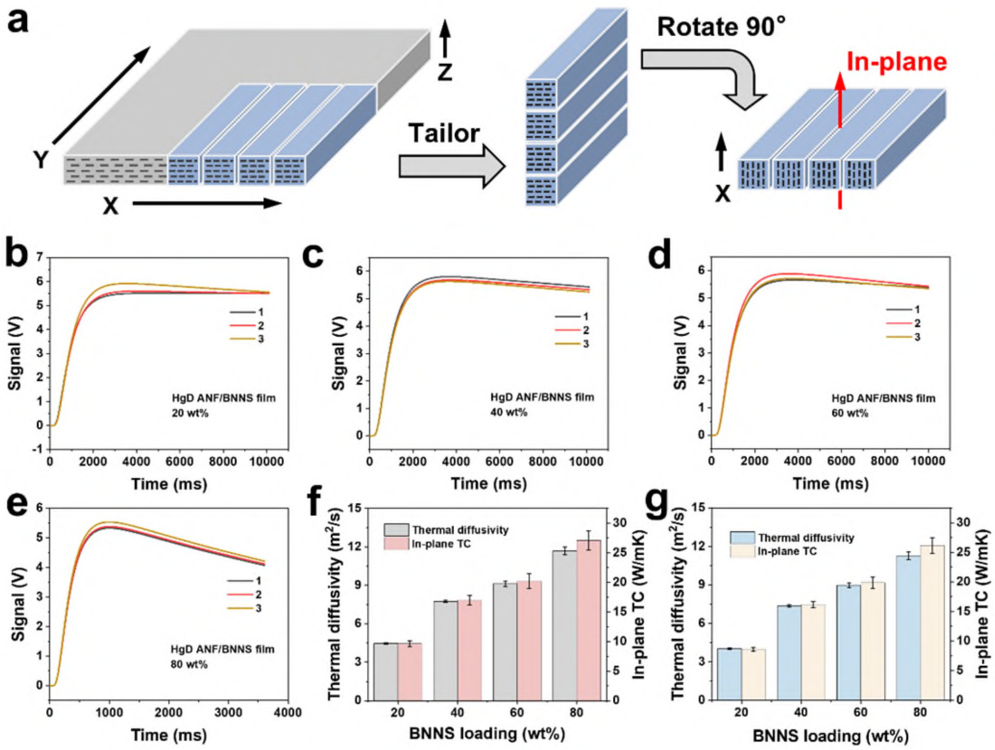

Figure R5. (a) Preparation of the ANF/BNNS films for measuring in-plane thermal diffusivities by a laser flash method. (b-e) The curves of the temperature (detector signal) increase over time obtained by the laser flash method. Comparison of Thermal diffusivities and conductivities of the HgD ANF/BNNS films tested by (f) this through-plane testing approach and (g) laser flash method.

4. There are no density and specific heat capacity data in the manuscript which are used to calculate thermal conductivity. The authors only claim specific heat capacity was evaluated via DSC measurements, without showing the DSC curves. However, DSC method is tricky for extracting specific heat capacity data as the data can be greatly overestimated if the contact of the measured sample and instrument is not good enough. The authors need to demonstrate that their enhanced thermal conductivity data are not artifacts of overestimated specific heat capacity values.

Reply: We are very sorry that we haven't provided the relevant test data on density and heat capacity. Density (ρ) was calculated based on the ratio of weight and volume measurements. The sample to be tested was first cut into a circular disc with a diameter of **25.4 mm** using standard cutter. The thickness (*d*) and weight of samples were measured using caliper and precision electronic balance, respectively. And the results were shown in Figure R6 (Supplementary Fig. 3b).

Revised in Supporting Information (Pages 4-5):

Measurement for density ρ

Density (ρ) was calculated based on the ratio of weight and volume measurements. The sample to be tested was first cut into a circular disc with a diameter of 25.4 mm using standard cutter. The thickness (d) and weight of samples were measured using caliper and precision electronic balance, respectively. And the results were shown in Supplementary Fig. 3b.

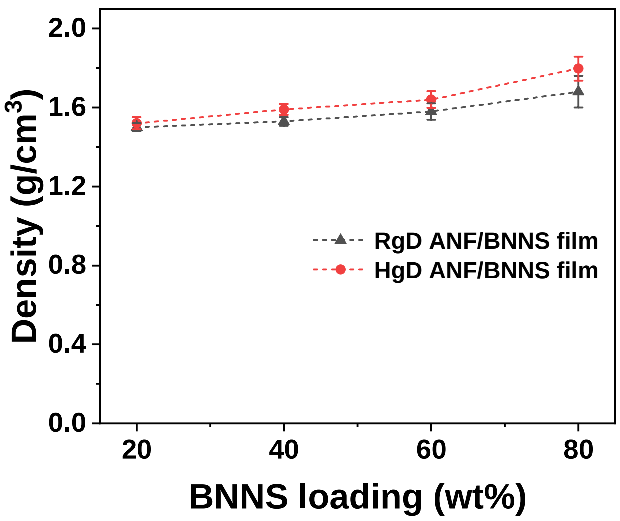

Figure R6 (Supplementary Fig. 3b). Density ρ of ANF/BNNS film with different BNNS loading.

Specific heat capacity C_p was evaluated by using differential scanning calorimeter (DSC Q2000, TA Instruments) measurements. The widely accepted DSC sapphire method (ISO 11357-4), which uses sapphire as the standard sample, can significantly improve the accuracy of C_p measurements obtained by DSC. As shown in Figure R7 (Supplementary Fig. 1), to minimize potential errors from inadequate contact between the sample and instrument during DSC testing for C_p measurement, each sample was tested 3 times, and the average value was calculated. To improve the accuracy of the heat flow curve, the difference between the starting/ending temperatures and the target specific heat temperature was set to 40 °C (>30 °C), with a constant temperature time of 10 min. Additionally, a higher heating rate (10 °C/min) and larger sample size were employed to ensure both the accuracy and precision of the measurement results. The C_p of the film was calculated based on the known C_p of sapphire.

$$C_{p\ Sample} = \frac{m_{Sapphire}}{m_{Sample}} \frac{(\Phi_{Sample} - \Phi_{blank\ run})}{(\Phi_{Sapphire} - \Phi_{blank\ run})} C_{p\ Sapphire} \quad \text{(R2)}$$

where m is the weight of the film, Φ_{Sample}, $\Phi_{Sapphire}$, $\Phi_{blank\ run}$ are DSC heat flow of the film, sapphire and empty crucible, respectively. The C_p of the films, as calculated using eq. R2, is presented in Figure R8 (Supplementary Fig. 2). Furthermore, the thermal conductivity (Figure R9 (Fig. 5 a-d)) of the ANF/BNNS films was calculated using $k = \rho \cdot C_p \cdot \alpha$ and is presented in Supplementary Table 1.

Revised in Supporting Information (Pages 2-3):

Measurement for Specific heat capacity C_p

Specific heat capacity C_p was evaluated by using differential scanning calorimeter (DSC Q2000, TA Instruments) measurements. The widely accepted DSC sapphire method (ISO 11357-4), which uses sapphire as the standard sample, can significantly improve the accuracy of C_p measurements obtained by DSC. The C_p of ANF/BNNS film can be calculated by…

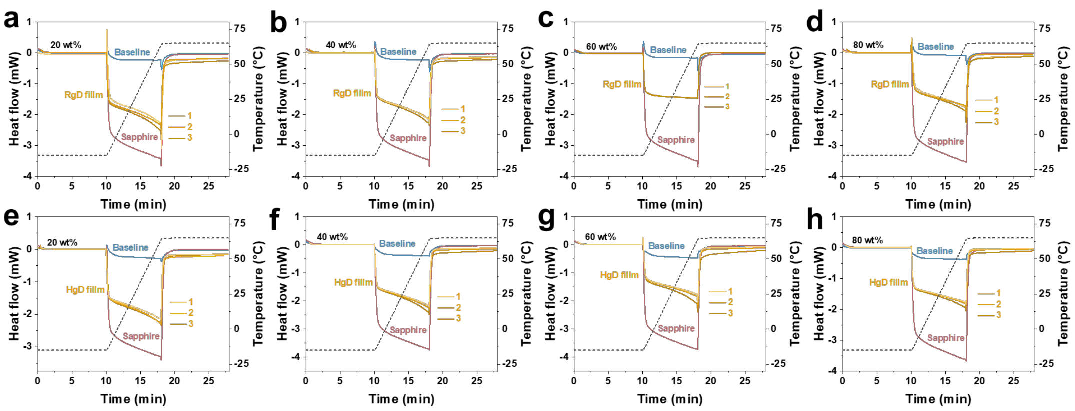

Figure R7 (Supplementary Fig. 1). DSC curves for specific heat capacity calculations: (a-d) RgD ANF/BNNS films and (e-f) HgD ANF/BNNS films.

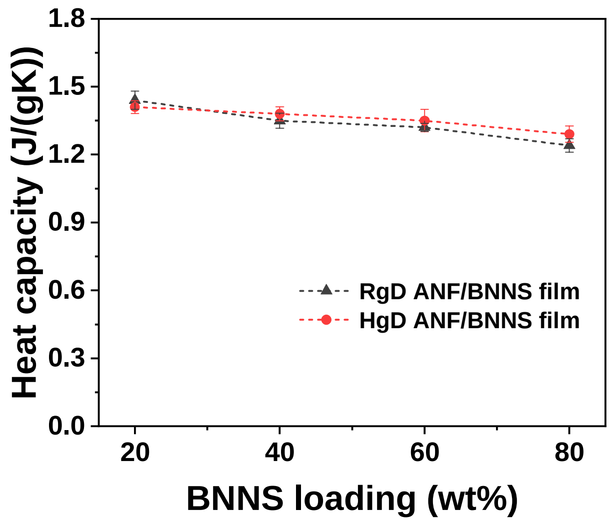

Figure R8 (Supplementary Fig. 2). Heat capacity measurements determined by DSC as a function of BNNS loading.

Revised in Manuscript (Page 11):

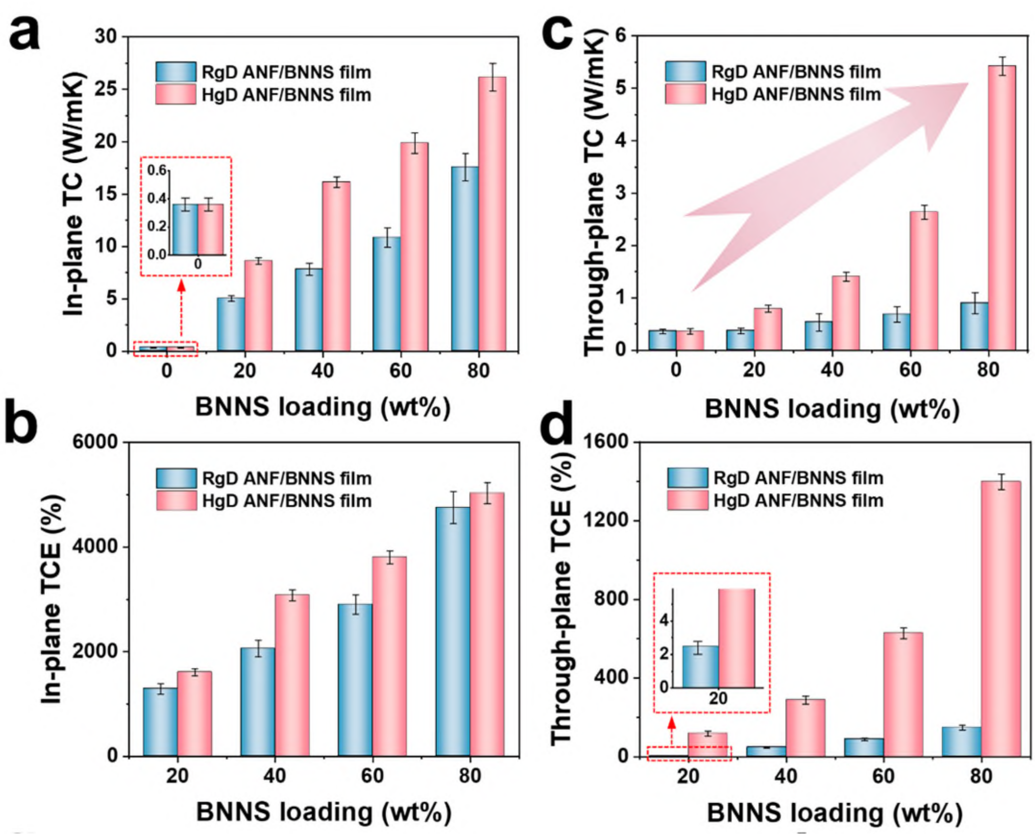

Figure R9 (Fig. 5 a-d). (a-d) Thermal conductivity and corresponding thermal conductivity enhancement of RgD and HgD ANF/BNNS films.

Revised in Supporting Information (Page 24):

Table R1 (Supplementary Table 1). Thermal diffusivity (α), Density (ρ), specific heat capacity (C_p) and thermal conductivity (TC) of the films.

Sample		In-plane α (mm^2/s)	Through-plane α (mm^2/s)	ρ (g/cm^3)	C_p (J/gK)	In-plane TC (W/mK)	Through-plane TC (W/mK)
RgD film	20 wt%	2.33	0.172	1.51	1.44	5.03	0.371
	40 wt%	3.78	0.258	1.53	1.35	7.82	0.533
	60 wt%	5.22	0.327	1.58	1.32	10.88	0.683
	80 wt%	8.61	0.432	1.68	1.24	17.57	0.899
HgD film	20 wt%	4.02	0.369	1.52	1.41	8.61	0.79
	40 wt%	7.36	0.641	1.59	1.38	16.16	1.405
	60 wt%	8.97	1.189	1.64	1.35	19.88	2.634
	80 wt%	11.27	2.339	1.79	1.29	26.16	5.425

5. In Fig. 6d and Fig. S19, why do the temperature differences between RgD and HgD films at radiation intensities of 50 mW/cm^2 and 200 mW/cm^2 increase with time, while those at 100 and 150 mW/cm^2 decrease?

Reply: We apologize for the confusion caused by the inadequate testing duration, which led to the sample temperatures from reaching a stable state across varying radiation intensities. By extending the test duration to 3600 s, a distinct plateau in the saturation temperature becomes observable (Figures R10-R12), while simultaneously avoiding the inconsistency of the temperature difference between RgD and HgD films under different radiation intensities. The revised real-time cooling performance and corresponding temperature statistical charts are displayed in revised manuscript Fig. 6c-e and revised supporting information Supplementary Fig. 34 and Fig. 36.

Revised in Manuscript (page 17):

…As shown in Fig. 6c and d, covering the ANF/BNNS film effectively lowered the ambient temperature from 40.2 to 36.2 °C with an increasing BNNS content (from 20 to 80 wt%)…

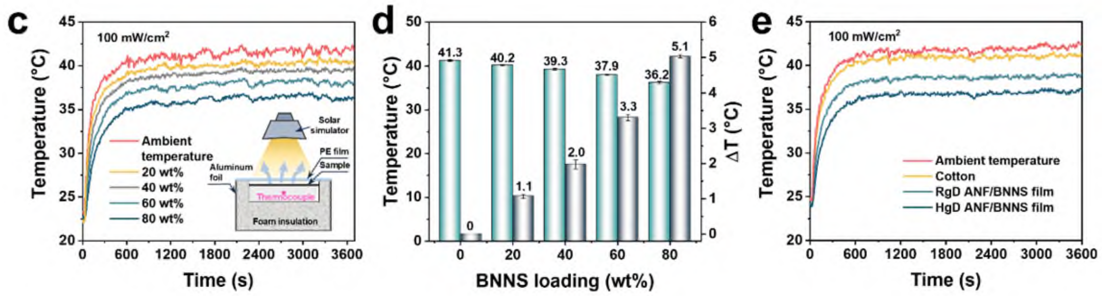

Figure R10 (Fig. 6c-e). (c) Schematic of experimental setup, real-time cooling performance and (d) corresponding temperature statistical charts of HgD ANF/BNNS films, (e) real-time cooling performance of different samples under simulated solar radiation (100 mW/cm^2).

Revised in Supporting Information (page 22):

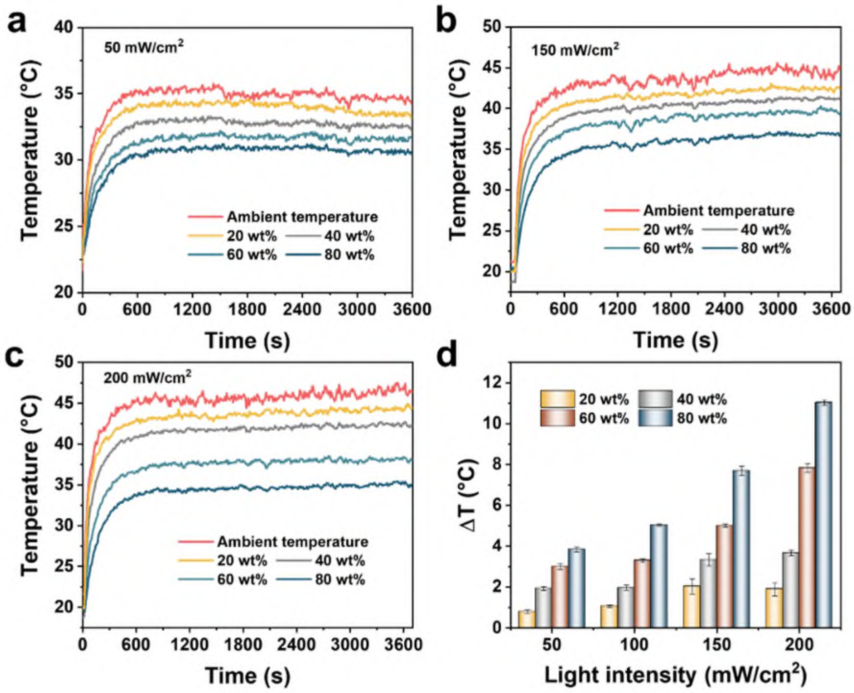

Figure R11 (Supplementary Fig. 34). (a-c) Temperature profiles of HgD ANF/BNNS films under different radiation intensity and (d) statistical analysis of the corresponding temperature differences.

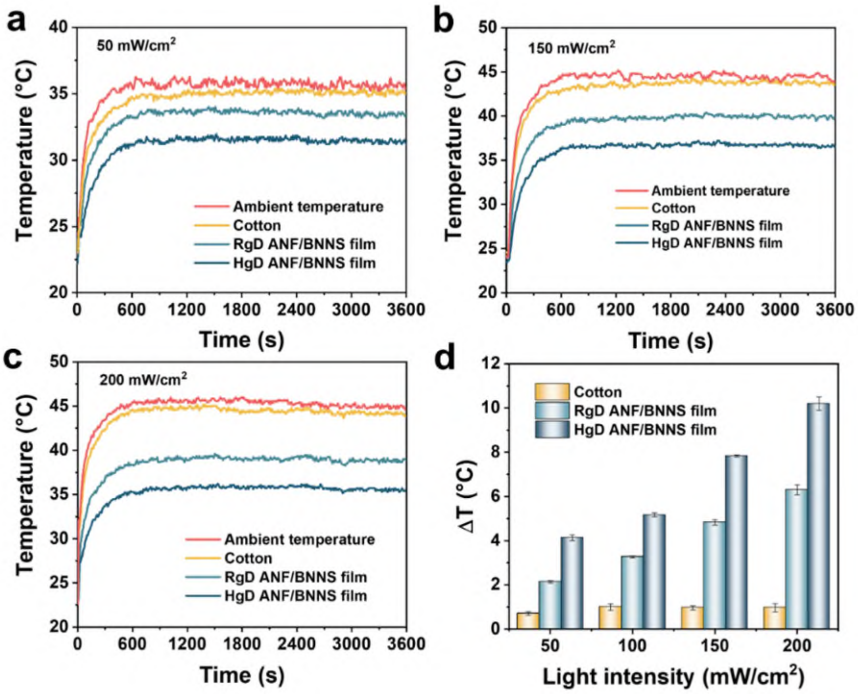

Figure R12 (Supplementary Fig. 36). (a-c) Temperature profiles of ambient air, cotton, RgD and HgD ANF/BNNS films under different radiation intensity and (d) statistical analysis of the corresponding temperature differences.

6. Several abbreviations, such as DSC and DTG, are used without being defined.

Reply: Thanks very much for your kind reminding. Based on your advice, we have added accordingly the full name of "DSC" and "DTG" at Characterizations section at page 21 in the revised manuscript.

Reviewer #2 (Remarks to the Author):

I co-reviewed this manuscript with one of the reviewers who provided the listed reports. This is part of the Nature Communications initiative to facilitate training in peer review and to provide appropriate recognition for Early Career Researchers who co-review manuscripts.

Reply: We appreciate your careful examination and helpful suggestion. As suggested, the manuscript has been carefully revised and the relevant changes are highlighted.

Reviewer #3 (Remarks to the Author):

This manuscript presents a novel honeycomb-gel densification (HgD) strategy to enhance the through-plane thermal conductivity in layered film-based thermal management materials (f-TMMs), by introducing interlayer phonon bridges via a carefully controlled freeze-casting and densification process. The integration of boron nitride nanosheets (BNNS) and aramid nanofibers (ANF) results in a bi-directional thermal conduction network, with reported enhancements in through-plane thermal conductivity surpassing many existing BNNS-based films. Additionally, the paper suggests a potential application in passive radiative cooling, demonstrating a temperature reduction of up to 10 °C under solar irradiation. While the work presents a promising approach with some strong experimental results, several critical aspects require further clarifications or study:

Reply: We appreciate your careful examination and helpful suggestion. As suggested, the manuscript has been carefully revised and the relevant changes are highlighted.

1. The process of freeze casting followed by gel densification is central to the study. How reproducible is this fabrication method? Are there any potential challenges in maintaining structural consistency across different batches?

Reply: Thank you for your questions. In this study, zigzag yet continuous interlayer phonon bridges within layered structures were successfully constructed via a honeycomb-gel densification strategy that integrates freeze-casting and gel densification. To evaluate the reproducibility of this fabrication method, we prepared five batches of composite films and systematically characterized their key properties, including sample morphology, internal microstructure, and thermal conductive performance.

Figure R13 (Supplementary Fig. 21) illustrates the preparation procedure of HgD ANF/BNNS films, where each batch contains of three individual films, demonstrating excellent film-forming stability of the preparation method. In the gradual densification of the ANF/BNNS hydrogel skeleton, the channels become deformed and flattened until the upper and lower layers make contact. SEM analysis of the cross-sectional microstructures of HgD ANF/BNNS films in different directions reveals that the top view exhibits a wavy and dense interlayer phonon bridging network (Figure R14, Supplementary Fig. 22). In contrast, the side view demonstrates a highly oriented laminar structure with well-defined alignment in the lateral direction (Figure R15, Supplementary Fig. 23). It is worth noting that the HgD ANF/BNNS films from different batches display highly consistent lamellar structures in the same orientation, which demonstrates the excellent reproducibility of the preparation method in constructing anisotropic layer structures. In terms of thermal conductive performance, the similar layered structure establishes nearly identical thermal conduction pathways in both the through-plane and in-plane directions, leading to an extremely limited variation in thermal conductivity (Figure R16, Supplementary Fig. 24). Based on the above results, it is confirmed that this fabrication method exhibits outstanding reproducibility.

To ensure structural consistency across different batches, two primary challenges must be addressed. First, during the thawing-gelation process, ANF/BNNS frozen blocks should be placed in a pre-cooled protonated solution to prevent internal melting, which could otherwise compromise the integrity of the honeycomb skeleton structure. Second, during the gel densification process, the molding pressure should be appropriately controlled to avoid cracking of the gel block during densification.

Revised in Manuscript (Page 9):

…In addition, HgD ANF/BNNS films from different batches consistently exhibited excellent film-forming performance, uniform top-view and side-view microscopic morphological characteristics, and comparable thermal conductivity, thereby confirming the high reproducibility of the gel densification strategy (Supplementary Figs. 21-24)…

Revised in Supporting Information (Supplementary Figs. 21-24):

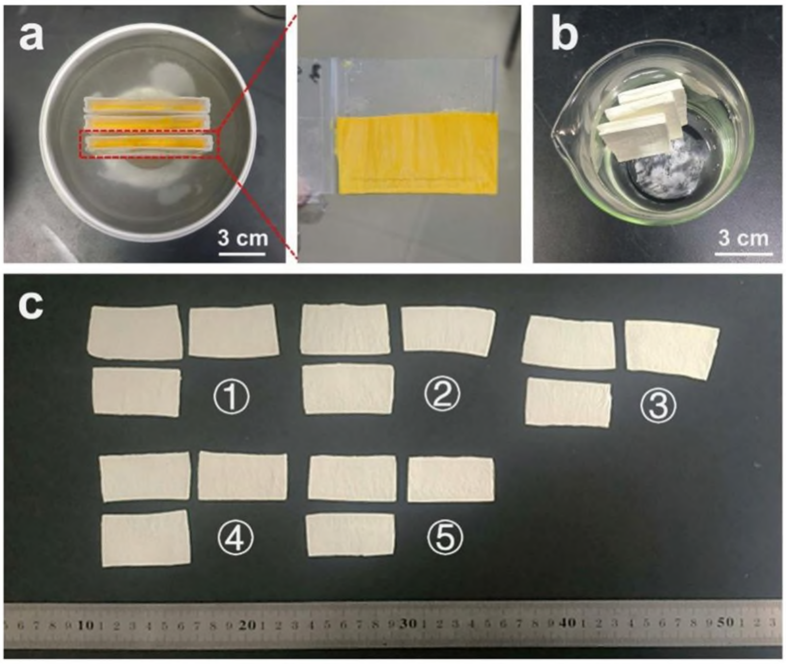

Figure R13 (Supplementary Fig. 21). The preparation of HgD ANF/BNNS films involve (a) freeze-casting and (b) thawing-gelation process. (c) Digital images of five batches of HgD ANF/BNNS films.

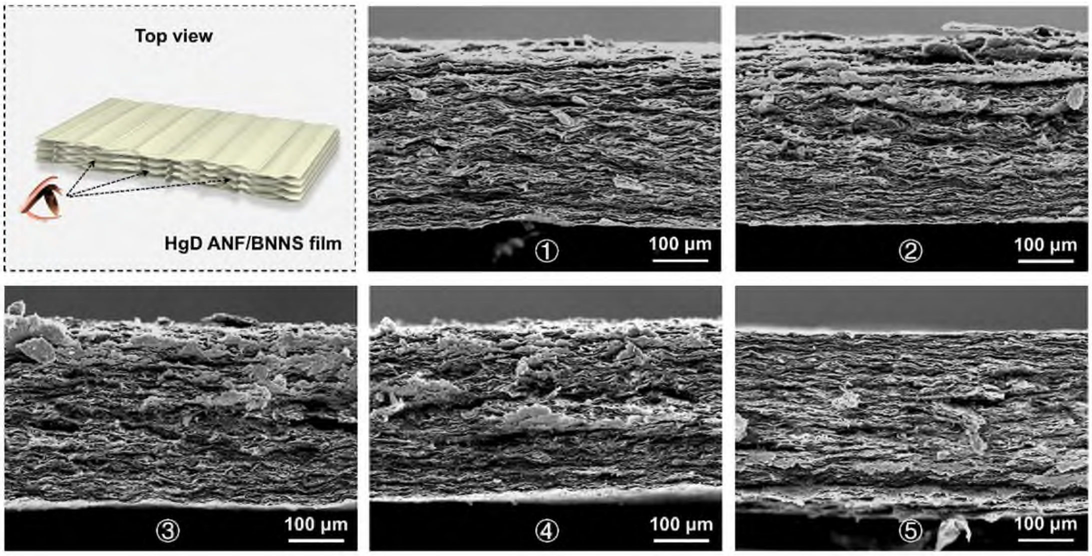

Figure R14 (Supplementary Fig. 22). Schematic diagram for the cross-sectional structure of HgD ANF/BNNS film and its cross-sectional morphology.

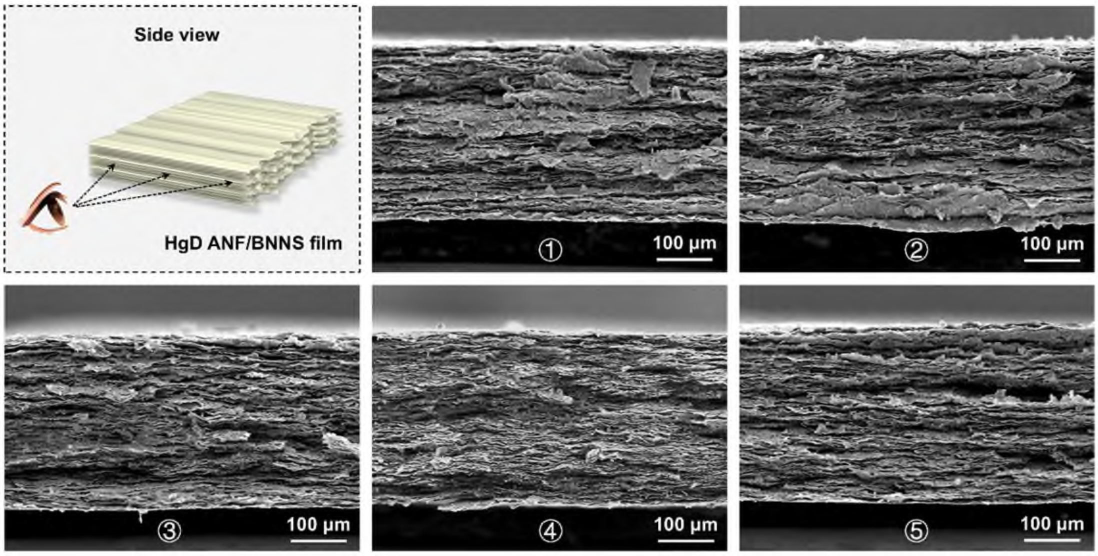

Figure R15 (Supplementary Fig. 23). Schematic diagram for the longitudinal structure of HgD ANF/BNNS film and its longitudinal morphology.

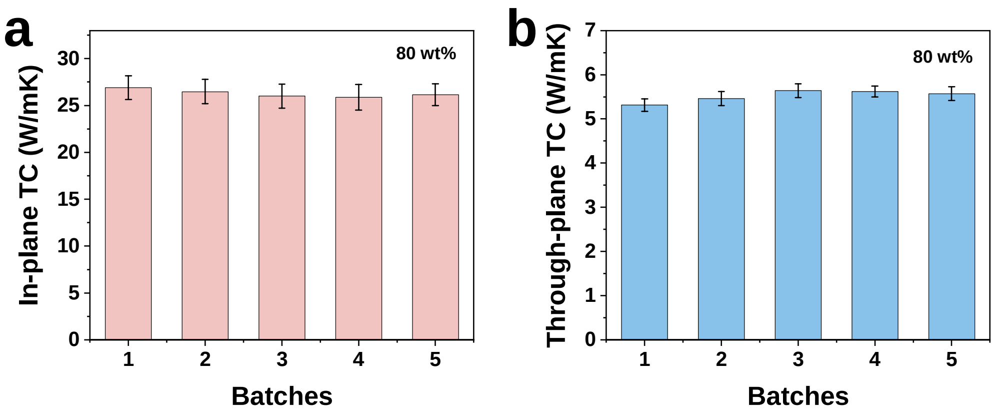

Figure R16 (Supplementary Fig. 24). The (a) in-plane and (b) through-plane thermal conductivities of HgD ANF/BNNS films of different batches.

2. The paper describes unidirectional freezing to form a honeycomb-likes skeleton. How sensitive is this structure to variations in freezing rate, solvent choice, or environmental conditions?

Reply: Thank you for your question. To evaluate the sensitivity of the formation of honeycomb-like skeletons during unidirectional freezing to the freezing rate and changes in environmental conditions, the corresponding skeleton morphologies were observed respectively. Notably, in this study, the DMSO solution of ANF/BNNS was used for unidirectional freezing, and the ANF/BNNS gel blocks with honeycomb skeleton structures were prepared via the solvent exchange between DMSO and H_2O, leveraging the gelation ability during the protonation process of ANF. Since DMSO was fixed as the solvent in the experiments, the impact of solvent choice on the skeleton structures was not further investigated.

To investigate the effect of freezing rate on the formation of the honeycomb framework, the freezing rate was effectively decreased by stacking 2 cm thick Cu blocks, which adjusted the freezing temperature (Figure R17a, Supplementary Fig. 12a). By placing 1, 2, or 3 Cu blocks in liquid nitrogen, the surface temperatures of the blocks were measured to be -171.2, -130.2, and -57.6 °C, respectively, using a thermometer (Figure R17b, Supplementary Fig. 12b). The ANF/BNNS solution was carefully poured into a square mold positioned above the Cu block. Under the influence of the freezing gradient, a honeycomb-skeleton structure was formed within the frozen block via the ice crystal growth process (Figure R17c, Supplementary Fig. 12c). Notably, when the surface temperature of the Cu block was relatively high, the freezing rate decreased significantly. When the freezing rate is relatively high (-171.2 and -130.2 °C), the ANF/BNNS network can be clearly observed using SEM technology. Along the crystal growth direction, this network exhibits a highly vertically aligned three-dimensional honeycomb channel structure (Figure R17 b_1-b_2' (Supplementary Fig. 12 b_1-b_2')). Under varying freezing rate conditions, the resulting honeycomb structures display certain similarities. However, when the freezing rate is decreased (-57.6 °C), the ice crystals grow more slowly, which makes it challenging to precisely control the size of the ice crystal columns.

Furthermore, by modulating the temperature and humidity, the impact of environmental condition variations on the skeletal structures was systematically investigated. Under an ambient temperature of 23.6 °C, the temperature surrounding the freezing experiment was increased to 41.2 °C and 65.9 °C, respectively, by modulating the heater power (Figure R18a-c (Supplementary Fig. 13)). By observing the top and side cross-sections of the ANF/BNNS frozen blocks (Figure R18a_1-c_2), it was found that they display a consistently honeycomb-like skeleton structure across varying environmental temperatures. This suggests that changes in environmental temperature have a limited influence on the formation of the skeleton structure. In addition, under an environmental humidity of 23.7% RH, a humidifier was used to continuously supply water vapor, thereby stabilizing the humidity surrounding the freezing experiment at 66.8% RH (Figure R19, Supplementary Fig. 14). Since the variation in environmental humidity does not influence the role of the low-temperature Cu block in promoting directional growth of the solution within the mold, the resulting skeleton structure exhibits consistency in both directions. The above results demonstrate that variations in environmental conditions, such as temperature and humidity, exert a minimal influence on the structure of honeycomb skeletons.

Revised in Manuscript (Page 7):

…It is worth noting that variations in freezing rate and environmental conditions (temperature and humidity), exert a minimal influence on the structure of honeycomb skeletons (Supplementary Figs. 12-14).

Revised in Supporting Information (Supplementary Figs. 12-14):

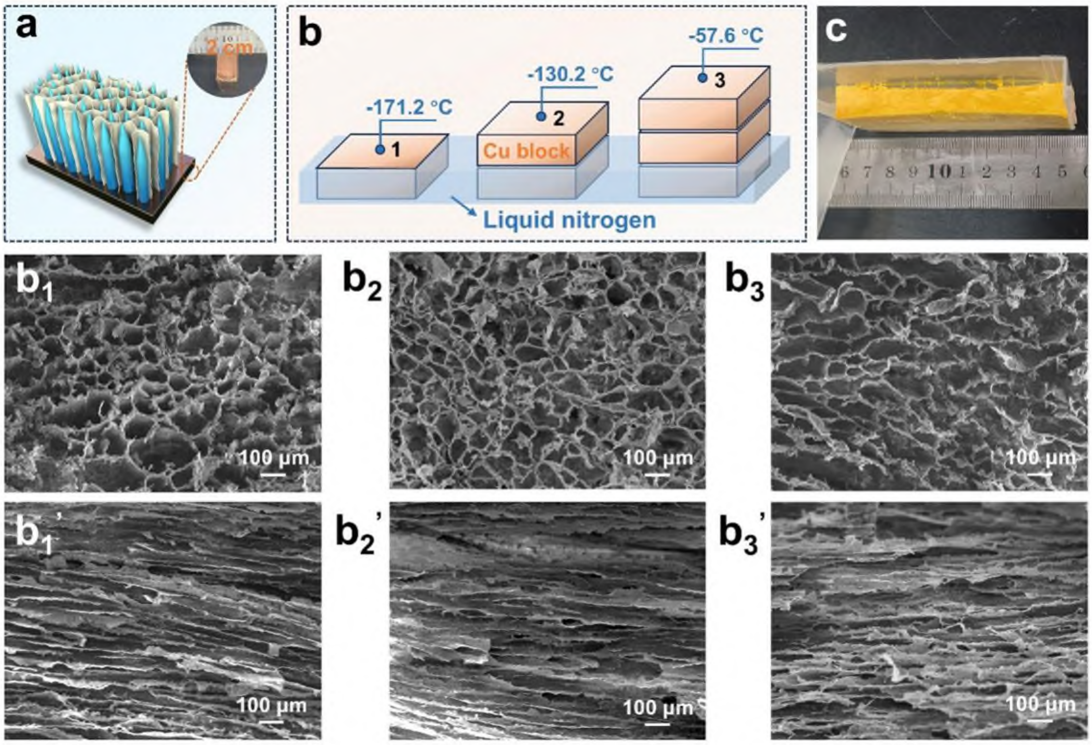

Figure R17 (Supplementary Fig. 12). The influence of freezing rate on the construction of honeycomb skeleton. (a) Schematic diagram of directional freezing. (b) Temperature distribution at different heights from the liquid nitrogen plane. (c)

Digital image of the ANF/BNNS frozen block. (b_1-b_3) Top and (b_1'-b_3') side view SEM images of ANF/BNNS skeleton under different freezing rates.

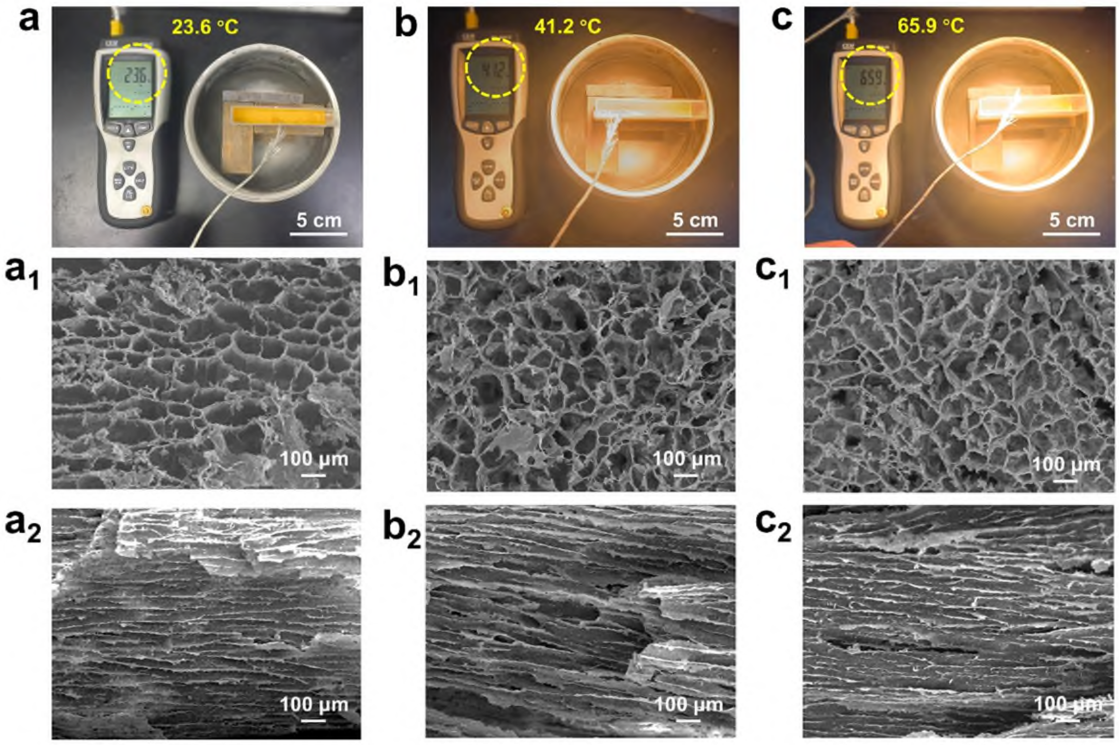

Figure R18 (Supplementary Fig. 13). The influence of environmental temperature on the construction of honeycomb skeleton. (a-c) Digital images of the freezing process under various environmental temperature conditions. (a_1-c_1) Top and (a_2-c_2) side view SEM images of ANF/BNNS skeleton under the corresponding environmental temperature conditions.

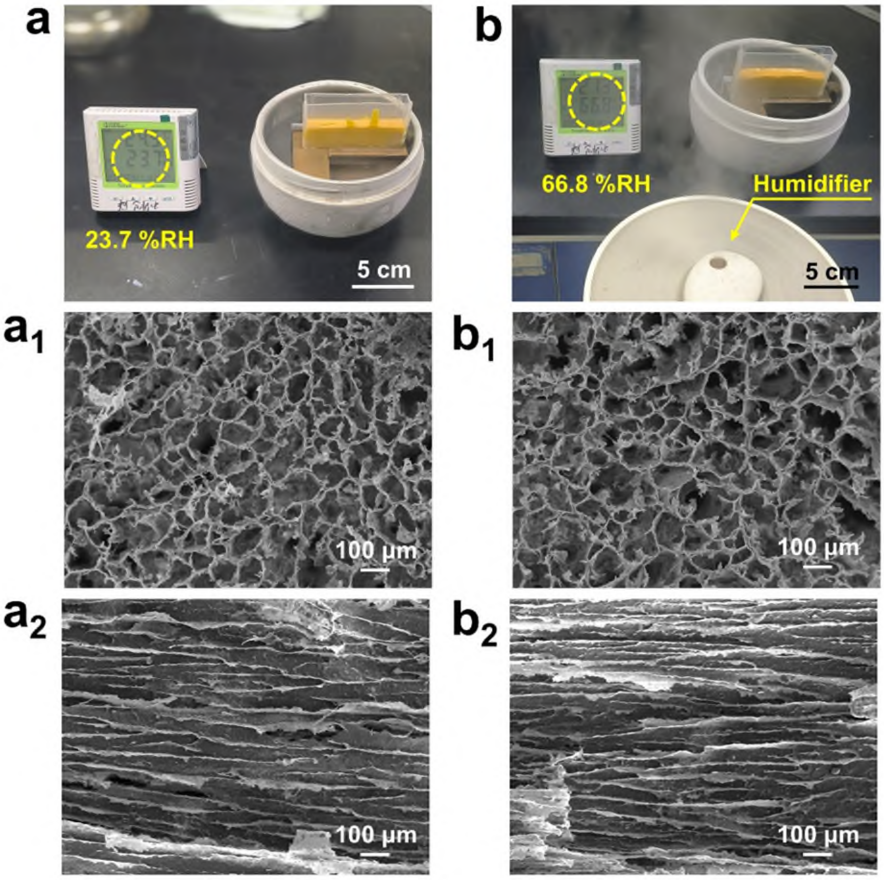

Figure R19 (Supplementary Fig. 14). The influence of environmental humidity on the construction of honeycomb skeleton. (a, b) Digital images of the freezing process under various environmental humidity conditions. (a_1, b_1) Top and (a_2, b_2) side view SEM images of ANF/BNNS skeleton under the corresponding environmental humidity conditions.

3. How does the applied pressure during densification affect the final film morphology and thermal performance? Is there an optimal pressure range that was determined experimentally?

Reply: Thank you for your questions. To investigate the effects of different pressures on the final morphology and thermal performance of films during gel densification, six pressure levels (2.5, 5, 10, 15, 20 and 25 MPa) were applied. As shown in Figure R20 (Supplementary Fig. 18), within the range of 2.5 to 15 MPa, the HgD ANF/BNNS films exhibited intact and smooth surface morphology. However, when the pressure was further increased beyond 20 MPa, cracks began to form in the gel membranes during densification. Especially, at 25 MPa, where obvious cracks led to the failure of film formation. The internal micro-layer structure of the composite membrane was further examined using SEM technology (Figure R21 (Supplementary Fig. 19)). At 2.5 MPa, significant pores were observed between the layers of the film, leading to an overall loose stacking structure. As the pressure progressively increased, the films exhibited a densely stacked structure with in-plane oriented BNNS in the side view, while in the top view, it presented a wavy and closely connected layered structure, with each layer being interconnected.

The thermal performance of the HgD ANF/BNNS film primarily depends on the formation of in-plane and through-plane thermal transport pathways within the material. However, at a relatively low pressure (2.5 MPa), incomplete thermal conduction pathways result in a lower thermal conductivity value (23.26 W/mK). In contrast, within the pressure range of 5-15 MPa, more complete thermal conduction pathways are formed, leading to significantly higher in-plane and through-plane thermal conductivities (Figure R22 (Supplementary Fig. 20)). Consequently, by systematically varying the pressure conditions and comprehensively evaluating factors such as final film morphology, microstructure, and thermal performance, the optimal pressure range for the ANF/BNNS film can be determined as 5-15 MPa.

Revised in Manuscript (Page 9):

…By systematically varying the pressure conditions and comprehensively evaluating factors such as final film morphology, microstructure, and thermal performance, the optimal pressure range for the ANF/BNNS film can be determined as 5-15 MPa (Supplementary Figs. 18-20).

Revised in Supporting Information (Supplementary Figs. 18-20):

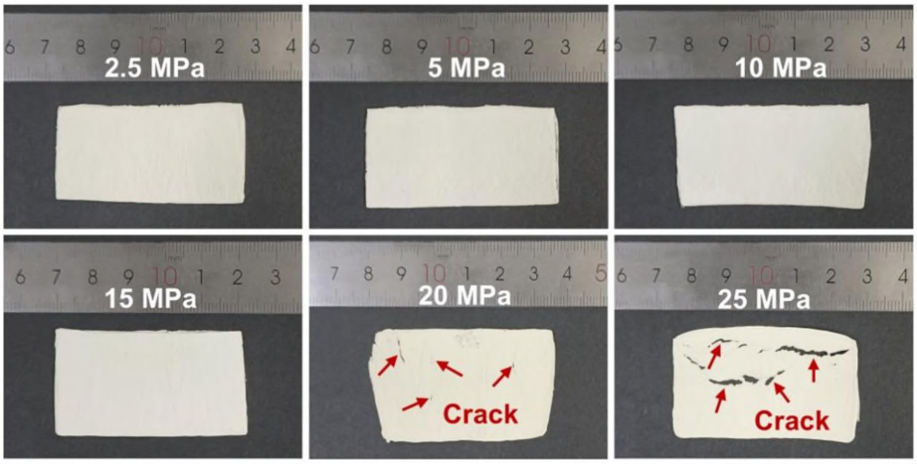

Figure R20 (Supplementary Fig. 18). The final film morphology obtained under varying pressures during the densification process.

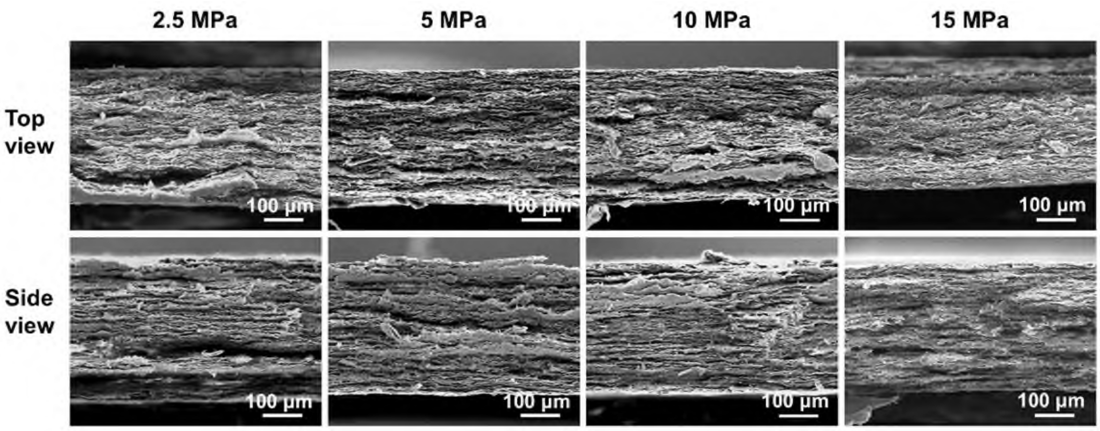

Figure R21 (Supplementary Fig. 19). SEM images of top and side views for HgD ANF/BNNS films under various pressures.

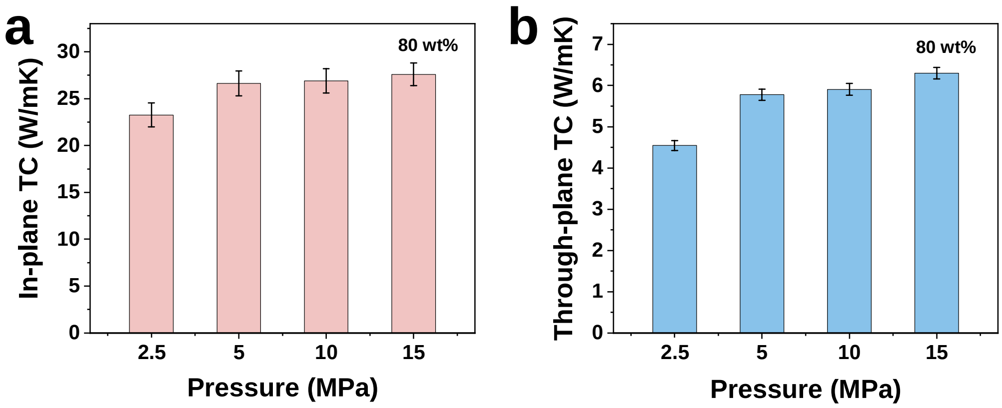

Figure R22 (Supplementary Fig. 20). The (a) in-plane and (b) through-plane thermal conductivities of HgD ANF/BNNS films of different pressure.

4. The anisotropy in thermal conductivity is discussed, with higher values in-plane compared to through-plane. How do the observed values align with theoretical predictions based on phonon transport models?

Reply: Thank you for your question. As suggested, we employed an effective medium approximation (EMA) model to theoretically predict the thermal conductivity (TC) of the material in both in-plane and through-plane directions. The EMA model is widely recognized as an effective approach for evaluating interfacial thermal resistance (Kapitza resistance) through experimental TC measurements. Conversely, under the assumption of negligible interfacial thermal resistance, this model can also be utilized to estimate the theoretical TC of composites. The general mathematical model of EMA theory is as follows:

$$K_{11}^{*}=K_{22}^{*}=K_m\frac{2+f[\beta_{11}(1-L_{11})(1+\langle\cos^2\theta\rangle)+\beta_{33}(1-L_{33})(1-\langle\cos^2\theta\rangle)]}{2-f[\beta_{11}L_{11}(1+\langle\cos^2\theta\rangle)+\beta_{33}L_{33}(1-\langle\cos^2\theta\rangle)]} \quad \text{(R3)}$$

$$K_{33}^{*}=K_m\frac{1+f[\beta_{11}(1-L_{11})(1-\langle\cos^2\theta\rangle)+\beta_{33}(1-L_{33})\langle\cos^2\theta\rangle]}{1-f[\beta_{11}L_{11}(1-\langle\cos^2\theta\rangle)+\beta_{33}L_{33}\langle\cos^2\theta\rangle]} \quad \text{(R4)}$$

$$\beta_{ii}=\frac{K_{ii}^{c}-K_m}{K_m+L_{ii}(K_{ii}^{c}-K_m)}, \qquad \langle\cos^2\theta\rangle=\frac{\int\rho(\theta)\cos^2\theta\sin^2\theta d\theta}{\int\rho(\theta)\sin^2\theta d\theta} \quad \text{(R5)}$$

For laminate composites (layered films) with a matrix containing parallel flat plate inclusions oriented perpendicular to the X_3 axis, $p\rightarrow 0$, $L_{11}=0$ and $L_{33}=1$, and $<\cos^2\theta>$ = 1, and thus Eqs. R3 and R4 can be simplified as:

$$K_{11}^{*}=K_{22}^{*}=(1-f)K_m+fK_p \quad \text{(R6)}$$

$$K_{33}^{*}=K_mK_p/[K_p-f(K_p-K_m-\alpha K_p)] \quad \text{(R7)}$$

where K_{11}^{*} K_{22}^{*} are the in-plane TC, K_{33}^{*} is the through-plane TC. K_m and K_p are the TC of filler and matrix, respectively. f is the volume fraction of filler. α is a dimensionless parameter ($\alpha=R_bK_m/d$, where R_b is interfacial thermal resistance and d is filler's thickness).

Based on the Eqs. R6 and R7, along with the specific parameters of ANF and BNNS, we present the theoretical prediction curves of in-plane TC and through-plane TC of the ANF/BNNS films, with an assumption of ideal interfacial thermal resistance. As shown in Figure R23, the experimental TC values exhibit a trend that aligns well with the theoretically predicted curves. In contrast, the experimental in-plane TC values are consistently lower than the theoretically predicted values, primarily due to the idealized assumptions in the theoretical models, which include infinite aspect ratios of the layers, perfect in-plane orientation, and negligible interfacial thermal resistance. Besides, the experimental through-plane TC values surpass theoretical predictions even without considering interface thermal resistance, mainly owing to the effectively established continuous interlaminar phonon transport network across ANF/BNNS film.

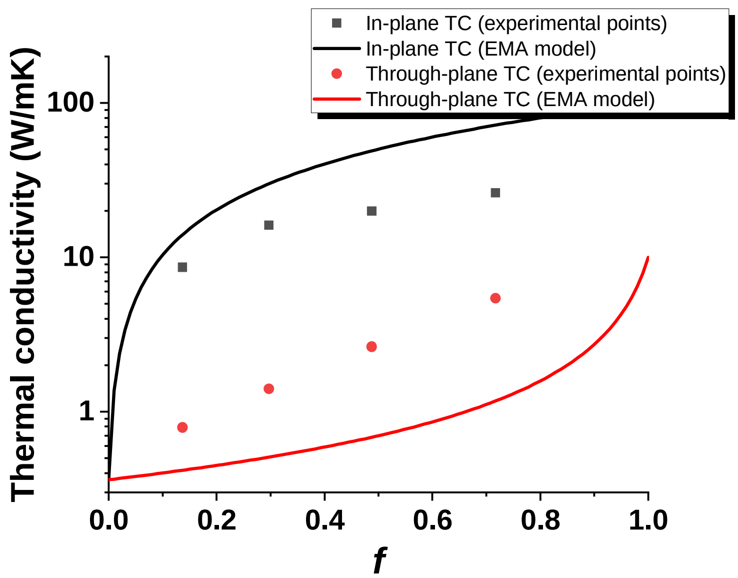

Figure R23. Experimental and theoretically predicted curves for the in-plane and through-plane thermal conductivities of ANF/BNNS films.

5. The discussion of interfacial phonon scattering suggests that ANF improves phonon transmission across BNNS layers. Are there any direct measurements of interfacial thermal resistance to support this hypothesis?

Reply: Thank you for your question. At present, it is still very difficult to directly test the interfacial thermal resistance between ANF and BNNS. Nevertheless, the analysis of phonon density of states (PDOS) predicted through the molecular chain models, according to the discrete Fourier transform of velocity autocorrelation function, can to some extent determine the interfacial thermal resistance between ANF and BNNS.

According to an important previous literature (*Adv. Mater.* 2020, 32, 1906939), the PDOS versus frequency results in Figure R24 manifested good phonon spectral match between h-BN and rigid ANF because of the extensive overlap regions, suggesting the efficient energy transfer and low phonon scattering at the BNNS–ANF interface.

Figure Redacted

Figure R24. The PDOS versus frequency results of h-BN and ANF. (Copyright 2020, Wiley-VCH, *Adv. Mater.* 2020, 32, 1906939).

6. The authors mention that the films exhibit flexibility. How does mechanical flexibility affect thermal performance, as well as durability in application?

Reply: Thank you for raising your question. To investigate the influence of mechanical flexibility on thermal performance, bending cycles were performed on the HgD ANF/BNNS film, and its thermal conductivity and application durability were systematically evaluated. After 5000 cycles of programmed controlled bending tests (Figure R25a (Supplementary Fig. 31a)), the results demonstrated that no damage occurred to the HgD ANF/BNNS film overall, suggesting its excellent flexibility. Owing to the film's excellent flexibility, the internal bidirectional heat conduction paths are preserved intact during the bending process. In comparison to the initial composite film with relatively high in-plane (26.06 W/mK) and through-plane (5.778 W/mK) thermal conductivity, after 5000 bending cycles, no significant alteration is observed in the thermal conductivity, where the in-plane thermal conductivity is 25.843 W/mK and the through-plane thermal conductivity is 5.472 W/mK (Figure R25b (Supplementary Fig. 31b)).

Durability is a critical factor for ensuring the reliability of HgD ANF/BNNS films in practical applications. For this purpose, the test samples before and after cyclic bending were individually employed as the thermal interface material (TIM) between a LED device and a cooling water heat sink, to assess their performance in heat dissipation management applications (Figure R25c-d (Supplementary Fig. 31c-d)).

Owing to the bidirectional heat dissipation capability of the HgD ANF/BNNS film, it enables effective uniform heat dissipation across the entire LED chip plane while significantly mitigating local overheating. Experimental results indicate that, in comparison to using the ANF film as the TIM, the surface temperature of the LED is further reduced by 35.8 °C. Notably, after undergoing 5000 bending cycles, the film continues to demonstrate heat dissipation performance equivalent to its initial state. The above results demonstrate that the excellent flexibility of the HgD ANF/BNNS film ensures its stable thermal performance, thereby enhancing its durability and reliability in practical applications.

Revised in Manuscript (Page 15):

…Owing to its excellent flexibility, notably, the HgD ANF/BNNS film retains its internal bidirectional thermal conduction pathways intact after 5000 bending cycles, with its thermal conductivity and heat dissipation performance remaining comparable to the initial state (Supplementary Fig. 31).

Revised in Supplementary Information (Supplementary Fig. 31):

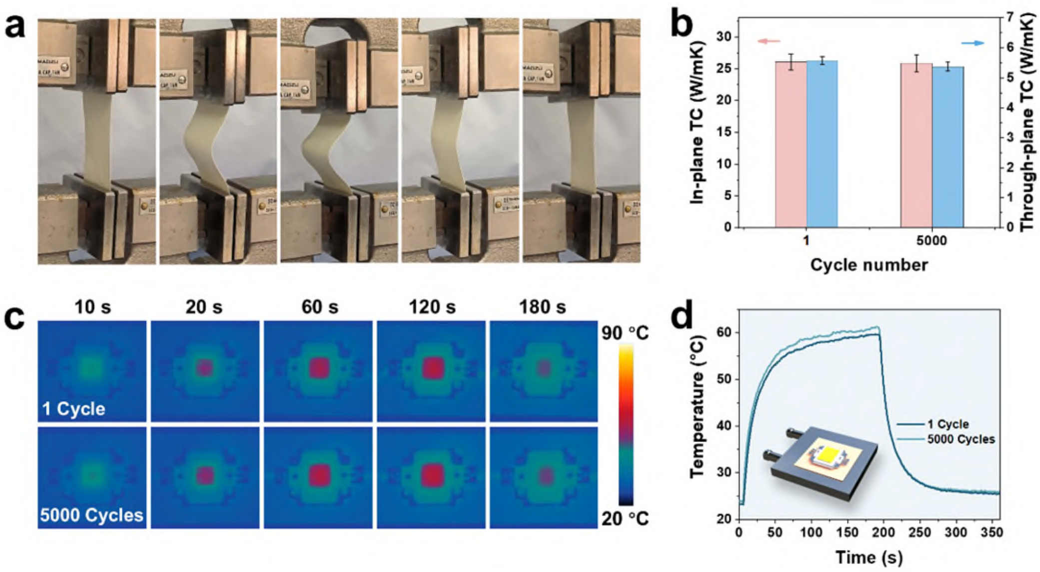

Figure R25 (Supplementary Fig. 31). (a) Photographs of the bending cycle process for HgD ANF/BNNS film. (b) Thermal conductivity of 5000 bending cycles of HgD ANF/BNNS film. (c) Infrared thermal images and (d) surface temperature profiles of HgD ANF/BNNS films as TIM between the LED chip and cooling water heat sink for heat dissipation application.

7. The authors showed the structural difference in the top view and the side view of the HgD ANF/BNNS film in Fig. 3(a, a', b, b'). It indicates different heat flow pathways in two directions in the in-plane, x and y, respectively, following the axis label in Fig. 3g. How does such structural difference affect the heat transfer in the x and y-direction? If a measurement technique that can distinguish the thermal conductivities in the two in-plane directions is not accessible, the author can visualize and demonstrate the heat conduction in the two directions using setups similar to those shown in Fig. 5 (a, b, e, f) and discuss the results.

Reply: Thank you for your professional comment. Based on your suggestion, the HgD ANF/BNNS film was cut into samples along the X and Y directions as indicated in the Figure R26a (Supplementary Fig. 28a). As shown in Figure 3a-b', the X direction exhibits a wavy and compact layered structure with interconnected layers, whereas the Y direction demonstrates a highly oriented and well-defined layered structure. Despite the structural differences observed in the HgD ANF/BNNS films between the X and Y directions, both them are classified as in-plane directions for the entire film. To visualize the practical heat transfer performance, similar to Fig. 5a and b, the X and Y directions films were vertically positioned on a hot plate, and the surface temperature distribution was recorded using an infrared camera (Figure R26b-c (Supplementary Fig. 28b-c)). The heat transfer rate from the bottom to the top of the membrane in both the X and Y directions exhibits minimal variability. Furthermore, upon reaching the final saturation temperature, the temperature gradient distributions along both directions are nearly identical.

Revised in Manuscript (Page 15):

…It is noteworthy that the HgD ANF/BNNS membranes exhibit a relatively minor difference in heat transfer rates along the in-plane X and Y directions (Supplementary Fig. 28).….

Revised in Supplementary Information (Supplementary Fig. 28)

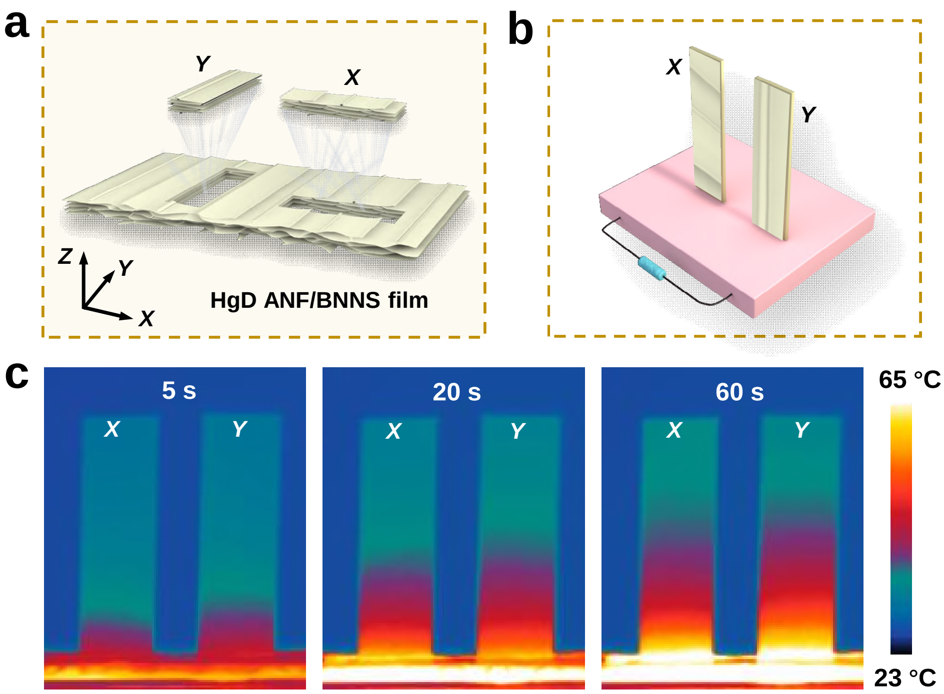

Figure R26 (Supplementary Fig. 28). (a) Schematic illustration of the sampling process for HgD ANF/BNNS films along the X and Y-direction. (b) Schematic of heat transfer demonstration set-up and (c) corresponding infrared thermal images.

8. How were the uncertainties in the thermal conductivity measurements analyzed? Error bars are missing in Fig.4 (a, c).

Reply: Thank you for your question and suggestion. The thermal conductivity (k) of the ANF/BNNS films can be calculated by the equation: $k = \alpha \times C_p \times \rho$, where thermal diffusivitiy (α) of the film was measured using LFA 467 NanoFlash system (NETZSCH, Germany), specific heat capacity (C_p) was evaluated by using differential scanning calorimeter (DSC Q2000, TA Instruments) measurements and density (ρ) was calculated based on weight and volume measurements. Therefore, the error bars in the thermal conductivity can be calculated by the errors in ρ, C_p and α (Figure R9 (Fig. 5 a-d)).

Thermal diffusivity α was measured using a laser flash apparatus (LFA467, NETZSCH). In accordance with the dimensions of the sample tray for the LFA 467 NanoFlash system, the sample to be tested was first cut into a circular disc with a diameter of 25.4 mm using standard cutter. Subsequently, the thickness (*d*) of samples were measured using caliper (Figure R1). Graphite was coated on the sample surface to minimize surface reflection and enhance laser energy absorption. At a constant temperature of 25 °C, a laser source emitted a pulse of light instantaneously and uniformly irradiated on the lower surface of the sample. The surface layer absorbed the light energy, causing an instantaneous temperature increase, which acted as the hot end to transfer energy to the cold end via one-dimensional heat conduction. An infrared detector is used to continuously measure the corresponding temperature rise in the center of the upper surface, and the temperature rise versus time curve is obtained (Figure R2). Thermal diffusivity values are measured at 3 points on the same specimen. The thermal diffusivity α can be calculated according to the eq. R1:

$$\alpha = \frac{0.1388d^2}{t_{50}} \quad \text{(R1)}$$

where d is the sample thickness and t_{50} is the characteristic time for the sample to heat up to the half of the maximum temperature. The thermal diffusivity values for different samples were calculated using equation (R1), as illustrated in Figure R3.

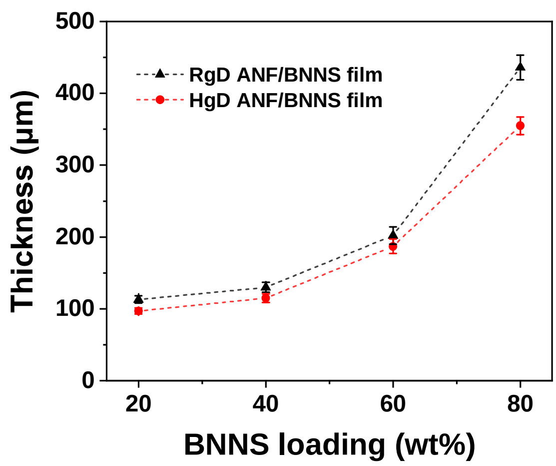

Figure R1 (Supplementary Fig. 3a). Thickness measurements determined by caliper as a function of BNNS loading.

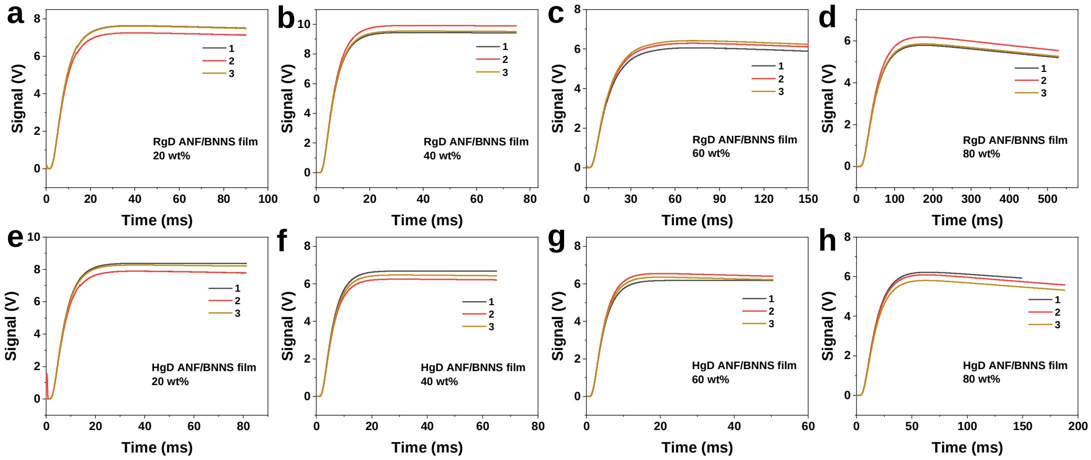

Figure R2 (Supplementary Fig. 4). The curves of the temperature (detector signal) increase over time obtained by the laser flash method.

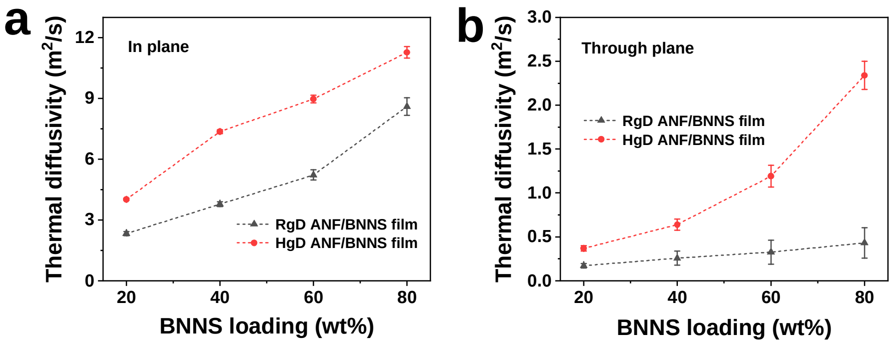

Figure R3 (Supplementary Fig. 5). Thermal diffusivity measured with a laser flash method (LFA467).

Specific heat capacity C_p was evaluated by using differential scanning calorimeter (DSC Q2000, TA Instruments) measurements. The widely accepted DSC sapphire method (ISO 11357-4), which uses sapphire as the standard sample, can significantly improve the accuracy of C_p measurements obtained by DSC. As shown in Figure R7 (Supplementary Fig. 1), to minimize potential errors from inadequate contact between the sample and instrument during DSC testing for C_p measurement, each sample was tested 3 times, and the average value was calculated. To improve the accuracy of the heat flow curve, the difference between the starting/ending temperatures and the target specific heat temperature was set to 40 °C (>30 °C), with a constant temperature time of 10 min. Additionally, a higher heating rate (10 °C/min) and larger sample size were employed to ensure both the accuracy and precision of the measurement results. The C_p of the film was calculated based on the known C_p of sapphire.

$$C_{p\ Sample} = \frac{m_{Sapphire}}{m_{Sample}} \frac{(\Phi_{Sample} - \Phi_{blank\ run})}{(\Phi_{Sapphire} - \Phi_{blank\ run})} C_{p\ Sapphire} \qquad \text{(R2)}$$

where m is the weight of the film, Φ_{Sample}, $\Phi_{Sapphire}$, $\Phi_{blank\ run}$ is DSC heat flow of the film, sapphire and empty crucible, respectively. The C_p of the composite films, as calculated using eq. R2, is presented in Figure R8 (Supplementary Fig. 2).

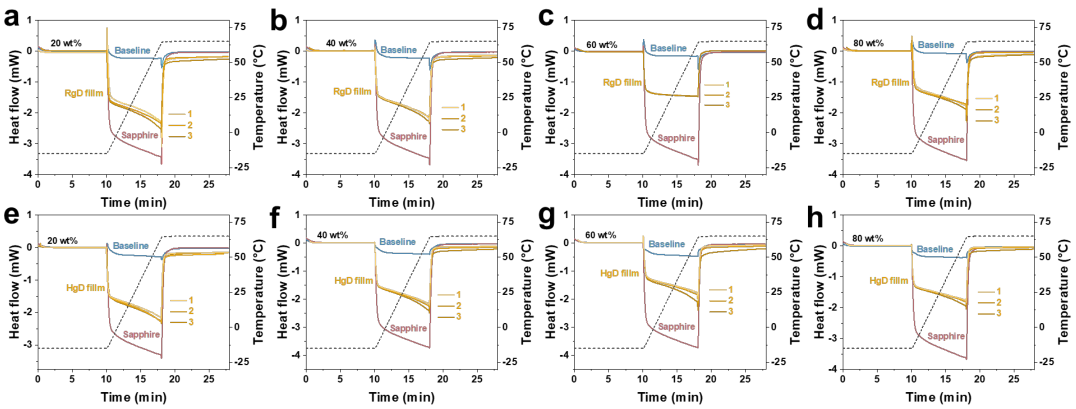

Figure R7 (Supplementary Fig. 1). DSC curves for specific heat capacity calculations: (a-d) RgD ANF/BNNS films and (e-f) HgD ANF/BNNS films.

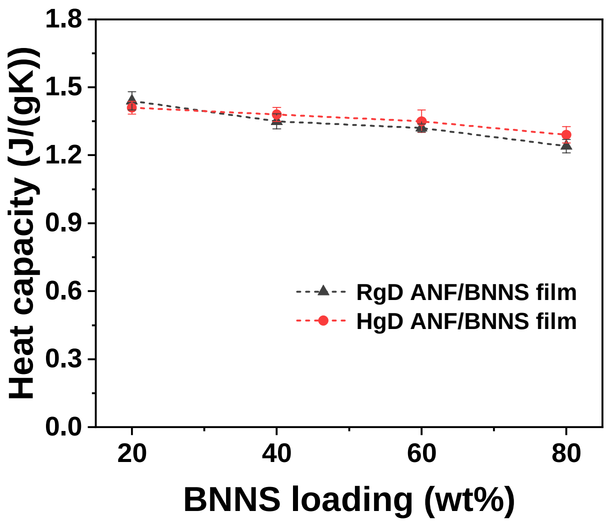

Figure R8 (Supplementary Fig. 2). (a) Heat capacity measurements determined by DSC as a function of BNNS loading.

Density (ρ) was calculated based on the ratio of weight and volume measurements. The sample to be tested was first cut into a circular disc with a diameter of **25.4 mm** using standard cutter. The thickness (d) and weight of samples were measured using caliper and precision electronic balance, respectively. And the results were shown in Figure R6 (Supplementary Fig. 3b).

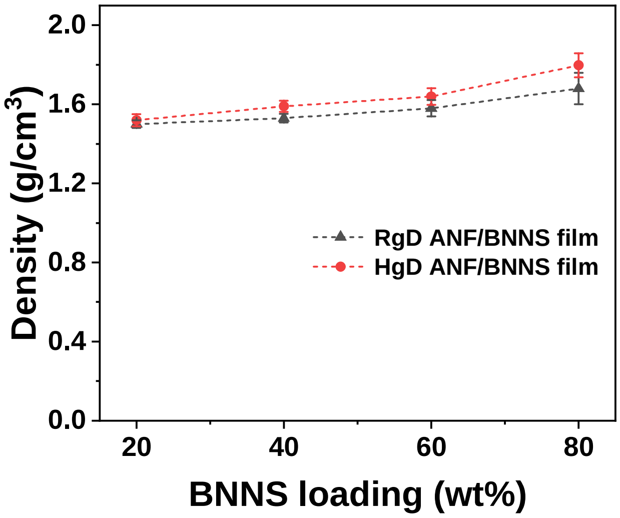

Figure R6 (Supplementary Fig. 3b). Density ρ of ANF/BNNS film with different BNNS loading.

Revised in Manuscript (page 11):

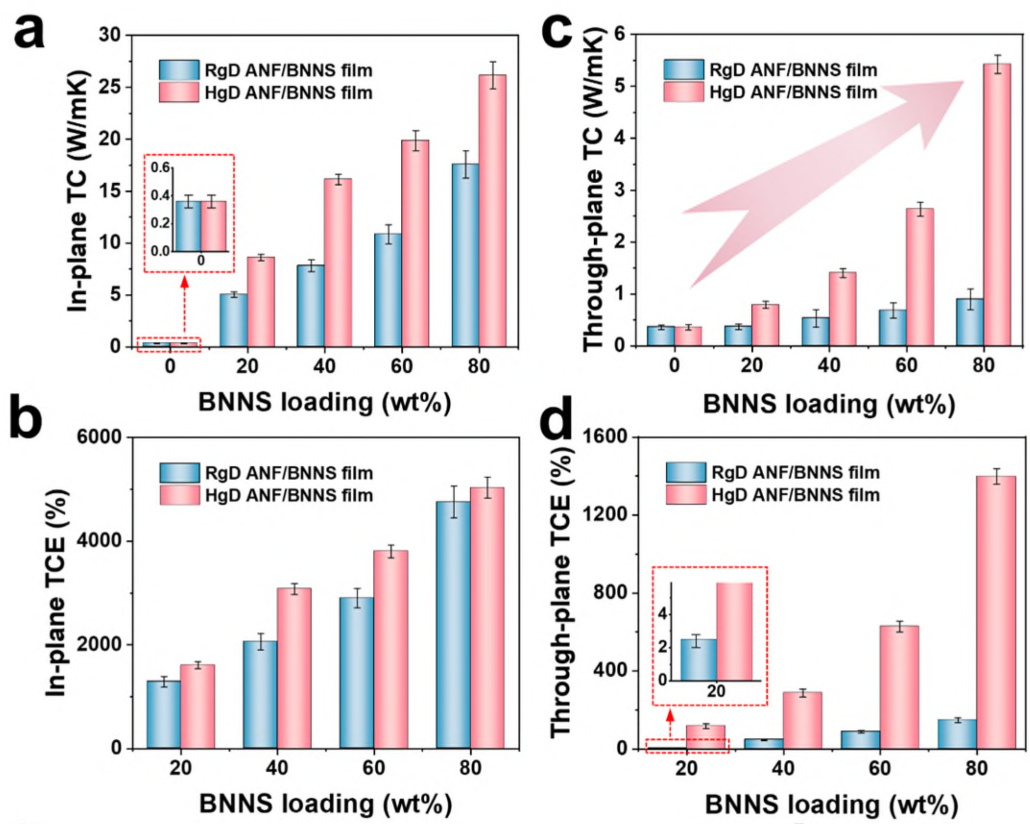

Figure R9 (Fig. 5 a-d). (a-d) Thermal conductivity and corresponding thermal conductivity enhancement of RgD and HgD ANF/BNNS films.

9. In Fig. 5f, is the top and bottom row showing the thermal images for RgD ANF/BNNS film and HgD ANF/BNNS film, respectively? Adding labels would avoid

confusion for the readers.

Reply: Thanks very much for your kind reminding. The top and bottom rows represent the thermal images of RgD ANF/BNNS film and HgD ANF/BNNS film, respectively, with the corresponding sample names clearly labeled (Figure R27 (Fig. 5f)).

Revised in Manuscript (Page 14):

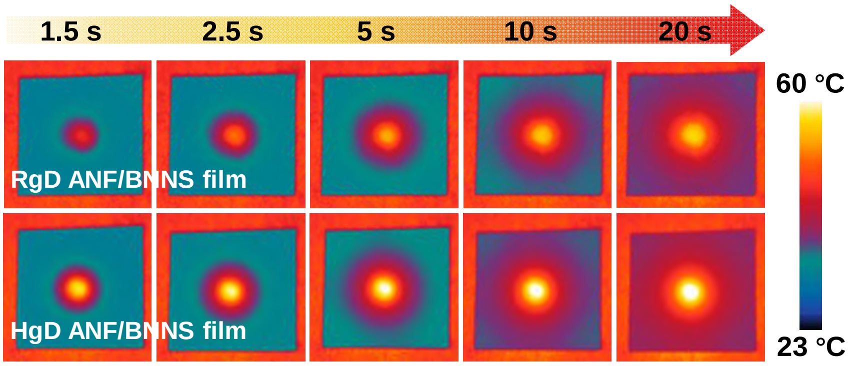

Figure R27 (Fig. 5f). Infrared thermal image of RgD ANF/BNNS film and HgD ANF/BNNS film under point heat source.

10. The authors briefly mentioned that they used insulating polystyrene foams and transparent polyethylene films to mitigate heat conduction and convection for the outdoor test. From the photo of the outdoor setup in Fig. 6g, I assume the polyethylene film covers the top of the setup. Wind can still cause strong forced convection for heat loss from the setup, which leads to unstable measurements. Tall wind shields around the setup may be a better option.

Reply: Thank you for your question. During the sub-environmental radiation cooling performance test, transparent polyethylene film was covered on the top of the outdoor setup, effectively reducing the influence of heat conduction and convection, thereby maximizing the accuracy of the test results (Figure R28a). To verify the critical role of covering the outdoor setup with a transparent polyethylene film in mitigating wind effects, uncovered installations were employed as the control group. As depicted in Figure R28b, when the device is directly exposed to the environment without PE film coverage, wind acts as the primary interfering factor. Specifically, variations in wind speed induce strong thermal convection, which markedly accelerates heat exchange between the setup surface and the surrounding air. This process leads to highly unstable temperature distribution, thereby causing significant fluctuations in measurement results. In contrast, wrapping the device with polyethylene film effectively mitigates these issues. The polyethylene film creates a transparent and efficient protective barrier around the setup, significantly reducing the thermal convection effect caused by wind. Consequently, this helps maintain the stability of the internal temperature of the setup and improves the accuracy and smoothness of the measurement results (Figure R28c). At present, in the majority of reported studies (*Nature, 2014, 515, 540-544, Science, 2024, 386,788-794, Nat. Commun., 2024, 15, 6100, Nat. Commun., 2023, 14, 6129.*), the common method to improving the setup is to cover it with a polyethylene film, and the ability of the sample in sub-environmental cooling performance is evaluated.

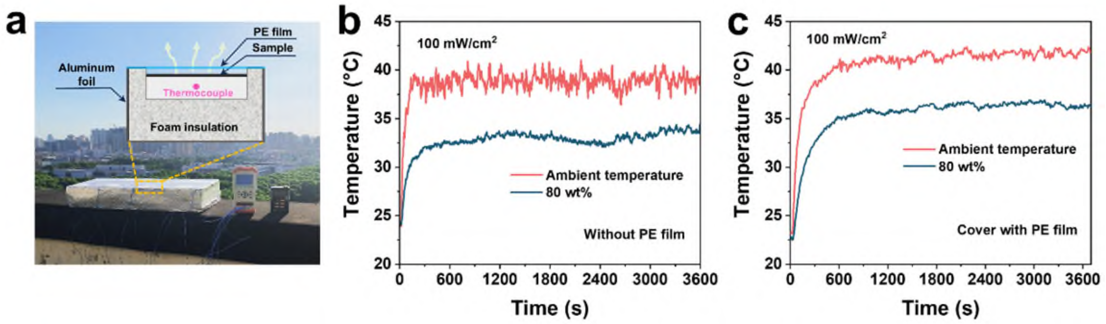

Figure R28. (a) Photograph and Schematic of subambient radiative cooling measurement setup. The real-time cooling performance of HgD ANF/BNNS films (b) without and (c) with PE film coverage.